Characterization of Mug33 reveals complementary roles for actin cable-dependent transport and exocyst regulators in fission yeast exocytosis

Hilary A. Snaith[1], James Thompson[2], John R. Yates, III[2] and Kenneth E. Sawin[1,*]

[1]Wellcome Trust Centre for Cell Biology, School of Biological Sciences, University of Edinburgh, Swann Building, Mayfield Road, Edinburgh EH9 3JR, UK
[2]The Scripps Research Institute, 10550 North Torrey Pines Road, La Jolla, CA 92037, USA
*Author for correspondence (ken.sawin@ed.ac.uk)

Accepted 5 March 2011
Journal of Cell Science 124, 2187-2199

doi:10.1242/jcs.084038

Summary

Although endocytosis and exocytosis have been extensively studied in budding yeast, there have been relatively few investigations of these complex processes in the fission yeast *Schizosaccharomyces pombe*. Here we identify and characterize fission yeast Mug33, a novel Tea1-interacting protein, and show that Mug33 is involved in exocytosis. Mug33 is a Sur7/PalI-family transmembrane protein that localizes to the plasma membrane at the cell tips and to cytoplasmic tubulovesicular elements (TVEs). A subset of Mug33 TVEs make long-range movements along actin cables, co-translocating with subunits of the exocyst complex. TVE movement depends on the type V myosin Myo52. Although *mug33*Δ mutants are viable, with only a mild cell-polarity phenotype, *mug33*Δ *myo52*Δ double mutants are synthetically lethal. Combining *mug33*Δ with deletion of the formin For3 (*for3*Δ) leads to synthetic temperature-sensitive growth and strongly reduced levels of exocytosis. Interestingly, mutants in non-essential genes involved in exocyst function behave in a manner similar to *mug33*Δ when combined with *myo52*Δ and *for3*Δ. By contrast, combining *mug33*Δ with mutants in non-essential exocyst genes has only minor effects on growth. We propose that Mug33 contributes to exocyst function and that actin cable-dependent vesicle transport and exocyst function have complementary roles in promoting efficient exocytosis in fission yeast.

Key words: Mug33, Actin filament, *Schizosaccharomyces pombe*, Sur7/PalI, Exocytosis, Fission yeast

Introduction

The interplay between actin filaments and subcellular vesicles is a key feature of membrane trafficking in yeast. Work in budding yeast from the 1970s onwards has identified many of the key molecules and mechanisms governing efficient endocytosis and exocytosis (Novick et al., 1980; Riezman, 1985), including several proteins regulating actin dynamics (Galletta and Cooper, 2009). During endocytosis, actin patches at the cell membrane are recruited to drive vesicle internalization (Gourlay et al., 2003; Huckaba et al., 2004; Kaksonen et al., 2003; Kubler and Riezman, 1993; Toshima et al., 2006). Once internalized, vesicles are transported on actin cables to an endosomal compartment (Huckaba et al., 2004). During exocytosis, actin cables are used for type V myosin-dependent transport of exocytic vesicles from the post-Golgi compartment to the plasma membrane (Govindan et al., 1995; Johnston et al., 1991; Pruyne et al., 1998; Schott et al., 2002; Trybus, 2008).

The exocyst, a multiprotein complex essential for polarized secretion in cell types from yeast to mammals, functions to tether exocytic vesicles at the plasma membrane before SNARE-mediated membrane fusion (He and Guo, 2009; Hsu et al., 2004; Hsu et al., 1996; Kee et al., 1997; Munson and Novick, 2006; TerBush et al., 1996; Wang et al., 2002; Wang and Hsu, 2006), which also involves the Sec1/Munc18 family of proteins (Scott et al., 2004; Shen et al., 2007; Toonen and Verhage, 2007; Wiederkehr et al., 2004). Budding yeast exocyst contains the subunits Sec3p, Sec5p, Sec6p, Sec8p, Sec10p, Sec15p, Exo70p and Exo84p and is required for all post-Golgi fusion events; mutations in exocyst components prevent growth of the daughter bud, assembly of the septin ring and cleavage of the septin ring at cell separation (He and Guo, 2009; Hsu et al., 1999). Most exocyst components are associated with exocytic vesicles, and this depends on the activated form of the Rab GTPase Sec4p, which binds to the Sec15p exocyst subunit (Boyd et al., 2004; Guo et al., 1999). Complete assembly of the exocyst takes place on the plasma membrane, where Sec3p and a portion of Exo70p are localized, independent of other subunits (He and Guo, 2009).

Fission yeast *Schizosaccharomyces pombe* grows in a highly polarized fashion, dependent on the actin cytoskeleton (Mitchison and Nurse, 1985; Rupes et al., 1999). Cell growth and division involves the polymerization of filamentous actin in a number of highly dynamic structures: membrane-associated patches, which are nucleated by the Arp2/3 complex and localize at sites of extensile growth at cell tips (McCollum et al., 1996); cytoplasmic actin cables nucleated at cell tips by the formin For3 (Feierbach and Chang, 2001; Feierbach et al., 2004); and the cytokinetic contractile ring, in which filaments are nucleated by the formin Cdc12 (Chang et al., 1997). Fission yeast initially grow in a monopolar fashion and then switch to bipolar growth after completion of S phase, in a process requiring redistribution of polarized actin [so-called ‘new-end take-off’ (NETO)] (Mitchison

and Nurse, 1985; Rupes et al., 1999). The trigger for this rearrangement of actin remains unclear, but it is dependent on the polarity regulator Tea1, perhaps through the proper activation of For3 at cell tips (Martin, 2009; Martin et al., 2005; Mata and Nurse, 1997).

Although there have been relatively few studies of endocytosis and exocytosis in fission yeast, the fundamental mechanisms of membrane trafficking in budding and fission yeasts appear to be similar (Gachet and Hyams, 2005; Wang, H. et al., 2003; Wang et al., 2002). Fission yeast endocytosis is actin-dependent and is restricted to sites of growth (i.e. at the cell tips and the cell-division site). Fission yeast also display polarized exocytosis, with exocytic vesicles directed to these same sites, and fission yeast homologues of the vesicle SNARE protein synaptobrevin (Syb1) (Edamatsu and Toyoshima, 2003), the exocyst complex (Wang, H. et al., 2003; Wang et al., 2002) and the Rab GTPase Sec4p (Craighead et al., 1993) have been characterized and shown to have roles in exocytosis similar to their budding yeast counterparts.

Despite these similarities, it is probable that there are also significant differences in membrane trafficking between budding and fission yeasts – for example, fission yeast does not contain an obvious homolog of Sec3p, and Exo70p is essential for viability in budding yeast but is non-essential in fission yeast (Wang, H. et al., 2003; Wang et al., 2002). This suggests that studies in fission yeast could reveal additional molecules and mechanisms regulating endocytosis and/or exocytosis (Sirotkin et al., 2010). Here, we describe a novel fission yeast transmembrane protein, Mug33, that localizes to cell tips and translocates along actin cables in tubulovesicular elements. Our characterization of Mug33 indicates that it contributes to exocyst function, and that efficient vesicle transport on actin cables and efficient exocyst function have complementary roles in promoting exocytosis in fission yeast.

Results

The Tea1-interacting protein Mug33 is a membrane protein associated with sites of cell growth

In a tandem-affinity purification of the cell-polarity regulator Tea1 (Mata and Nurse, 1997) we identified many known Tea1-interactors, including Tip1, Tea3, Tea4 and Mod5 (Fig. 1A) (Arellano et al., 2002; Brunner and Nurse, 2000; Martin et al., 2005; Snaith and Sawin, 2003), and several previously uncharacterized proteins, including Mug33 (SPCC1739.10; a complete list of proteins identified is presented in supplementary material Table S1). Mug33 (for meiotically-upregulated gene 33) was initially named as a result of a transcriptome analysis during meiosis (Mata et al., 2002). However, no meiotic defects have been identified in *mug33*Δ cells, which are viable (Gregan et al., 2005; Martin-Castellanos et al., 2005), and to date the function of Mug33 is unknown. We confirmed the Tea1–Mug33 interaction by co-immunoprecipitation (Fig. 1B).

Although *tea1*Δ mutants show a range of polarity defects, *mug33*Δ mutants showed minimal polarity defects. Unlike *tea1*Δ mutants, which grow in a monopolar fashion during exponential growth (Glynn et al., 2001; Mata and Nurse, 1997; Verde et al., 1995), *mug33*Δ cells grew in a bipolar fashion, like wild-type cells (supplementary material Fig. S1A, Fig. S4B), and *mug33*Δ cells were indistinguishable from wild-type cells by differential interference contrast (DIC) microscopy (supplementary material Fig. S4A). After stresses that transiently perturb the actin cytoskeleton, such as return-to-growth from stationary phase, up to 80–90% of *tea1*Δ cells form bent or branched cells (Browning et al., 2000; Sawin and Snaith, 2004; Snaith and Sawin, 2003). By contrast, in return-to-growth experiments *mug33*Δ cells grew as straight cells (Fig. 1C). Some mild polarity mutants in the Tea1 pathway, such as *mod5*Δ, grow as straight cells in conventional return-to-growth experiments but form bent or branched cells when return-to-growth experiments are performed in the presence of the microtubule-disrupting drug methyl benzimidizole-2-yl carbamate (MBC) (Snaith and Sawin, 2003). In return-to-growth experiments in the presence of MBC, *mug33*Δ mutants formed an intermediate number of bent or branched cells – greater than in wild-type cells but substantially less than in *mod5*Δ cells. (Fig. 1C). Overall, these results suggest that Mug33 plays a relatively minor role in growth–polarity regulation.

Mug33 is a 37-kDa protein that is alternatively predicted to contain either four transmembrane-spanning regions or a signal sequence and three transmembrane-spanning regions in its N-terminus; the Mug33 C-terminus (~150 amino acids) is predicted to be cytoplasmic. (Fig. 2A) (Bendtsen et al., 2004; Hofmann and Stoffel, 1993; Krogh et al., 2001). We identified obvious Mug33 primary sequence homologs in various *Schizosaccharomyces* species, with amino acid identity preserved along the length of the protein (supplementary material Fig. S1E). Database searching revealed that Mug33 is a member of the Sur7/PalI family (pfam 06687) of fungal transmembrane proteins, with similarity restricted to the N-terminus (Fig. 2A; supplementary material Fig. S1E). Budding yeast Sur7p, one of the more-studied members of this family, is a multicopy suppressor of mutations in the amphiphysins Rvs161p and Rvs167p,

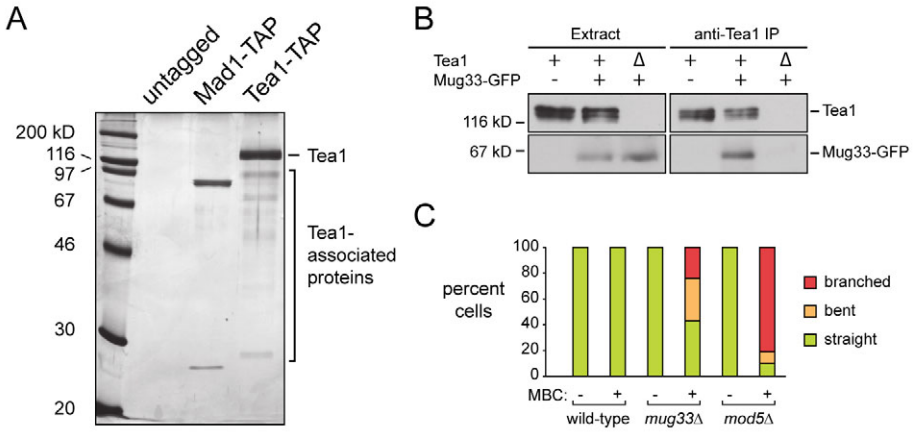

Fig. 1. Mug33 is a Tea1-interacting protein. (**A**) Silver-stained SDS-PAGE gel of TAP-purified Tea1, with TAP-purified Mad1 and mock-purification from untagged cells as negative controls. (**B**) Mug33–GFP co-immunoprecipitates with Tea1. Cell extracts and anti-Tea1 immunoprecipitates (IP) were probed with anti-Tea1 and anti-GFP antibodies. Δ indicates *tea1*Δ. (**C**) *mug33*Δ cells have only mild polarity defects. The percentage of straight, bent and branched cells in wild-type, *mug33*Δ and *mod5*Δ strains after polarity re-establishment in the presence and absence of the microtubule-depolymerizing drug MBC.

which are involved in the scission of endocytic vesicles (Kaksonen et al., 2005; Ren et al., 2006; Sivadon et al., 1997). Sur7p and its paralogs associate with eisosomes [which are also known as MCC (for membrane compartment of Can1p)], static membrane-associated protein complexes that have been implicated in sphingolipid metabolism, membrane organization and morphogenesis (Alvarez et al., 2008; Young et al., 2002). Eisosomes/MCC have been proposed to mark sites of endocytosis in budding yeast (Malinska et al., 2004; Walther et al., 2006), although recently this has been questioned (Brach et al., 2011; Grossmann et al., 2008). PalI is an *Aspergillus nidulans* protein (Rim9p in budding yeast) that serves as a transmembrane component of a signal transduction cascade sensing ambient pH (Calcagno-Pizarelli et al., 2007; Denison et al., 1998; Penalva et al., 2008). Whether the Sur7/PalI-conserved regions in these different proteins perform a specific or unique molecular function is currently unknown.

To study the dynamics of Mug33 localization, we tagged the chromosomal copy of the gene with GFP and examined its localization in wild-type cells and polarity mutants (Fig. 2B; supplementary material Fig. S2A). In wild-type interphase cells, Mug33–GFP was present in structures in the cytoplasm and on or near the plasma membrane at both cell tips. In dividing cells, Mug33–GFP was also enriched at the cell-division site (supplementary material Fig. S1B). In *tea1*Δ cells, Mug33–GFP was also found both in cytoplasmic structures and on the plasma membrane, but cell-tip localization was restricted to only one cell tip. This is probably a consequence of the monopolar growth of *tea1*Δ mutants rather than absence of Tea1 in itself, because we observed similar one-cell-tip localization in the monopolar-growth mutants *tea3*Δ, *bud6*Δ and *pak1-34* (Arellano et al., 2002; Glynn et al., 2001; Ottilie et al., 1995; Verde et al., 1995). Mug33 localization was relatively unaffected by deletion of the gene encoding the membrane-associated Tea1-binding protein Mod5, in which most cells undergo bipolar growth (Snaith and Sawin, 2003). Co-imaging of RFP-tagged Mug33 (Mug33–mKate) (Shcherbo et al., 2007; Snaith et al., 2010) together with actin filaments labeled with a GFP-tagged calponin homology domain of the IQGAP protein Rng2 (GFP–CHD^{Rng2}); (Karagiannis et al., 2005; Wachtler et al., 2003; Wang, C. H. et al., 2003) revealed that the one-cell-tip localization of Mug33 in *tea1*Δ cells was specific to the actin-rich growing end (Fig. 2C).

Because budding yeast Sur7 localizes to eisosomes/MCC, we examined the relationship between Mug33 and eisosomes/MCC, which has not been described in fission yeast to date. We tagged the fission yeast homolog of the budding yeast eisosome/MCC protein Pil1p with RFP (Pil1–tdTomato) and found that it localized to relatively immobile membrane-associated structures that are concentrated towards the cell middle (Fig. 2D,E) and are probably eisosome/MCC equivalents. We observed little or no overlap of Mug33–GFP with Pil1–tdTomato (Fig. 2E). To test whether the cytoplasmic C-terminal region of Mug33 was important for its localization, we generated a GFP-tagged version of Mug33 in which amino acids 181–336 are deleted but the Sur7/PalI-conserved region is left intact (Mug33ΔC–GFP). Interestingly, Mug33ΔC–GFP was no longer concentrated at cell tips but instead colocalized with Pil1–tdTomato (Fig. 2F,G). These results indicate that the Mug33 C-terminus is important for regulating Mug33 localization, perhaps overriding a PalI/Sur7 domain-driven association with an eisosome/MCC-like compartment.

Mug33 tubulovesicular elements translocate on actin cables using the type V myosin Myo52

Although we initially identified Mug33 as a Tea1-interacting protein, Mug33–GFP and Tea1–tdTomato showed only partial

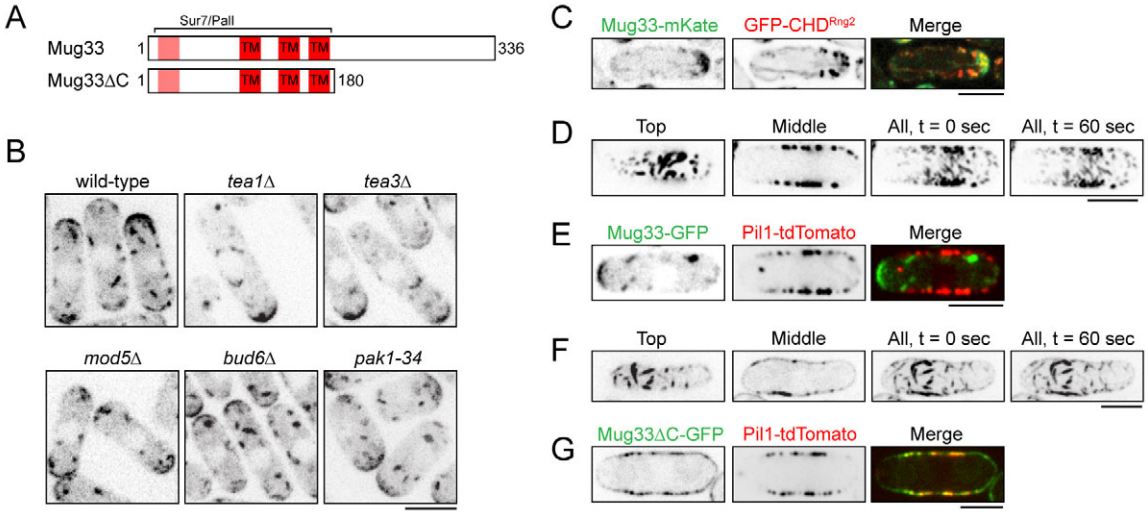

Fig. 2. Localization of Mug33 in wild-type and mutant cells. (**A**) Schematic diagram of full-length Mug33 and Mug33ΔC proteins, showing the position of transmembrane-spanning regions (red) and the Sur7/PalI-conserved region. The region indicated in pink is predicted to be either a transmembrane domain or a signal sequence, but this does not affect predicted membrane topology; in both cases the C-terminal tail of Mug33 is predicted to be intracellular. (**B**) Localization of Mug33–GFP in wild-type, *tea1*Δ, *tea3*Δ, *mod5*Δ, *bud6*Δ and *pak1-34* cells. (**C**) Colocalization of Mug33–mKate (green) with actin patches labeled by GFP–CHD^{Rng2} (red) in a monopolar *tea1*Δ cell. (**D**) Localization of Pil1–tdTomato to relatively immobile membrane-associated structures. The left-hand panels show top and middle *z*-sections, and right-hand panels show projections of all sections, 60 seconds apart. (**E**) A single *z*-section through a cell coexpressing Mug33–GFP (green) and Pil1–tdTomato (red), showing no apparent colocalization. (**F**) Localization of Mug33ΔC–GFP to relatively immobile membrane-associated structures. Labeling is as in D. (**G**) A single *z*-section through a cell coexpressing Mug33ΔC–GFP (green) and Pil1–tdTomato (red), showing significant colocalization. Scale bars: 5 µm.

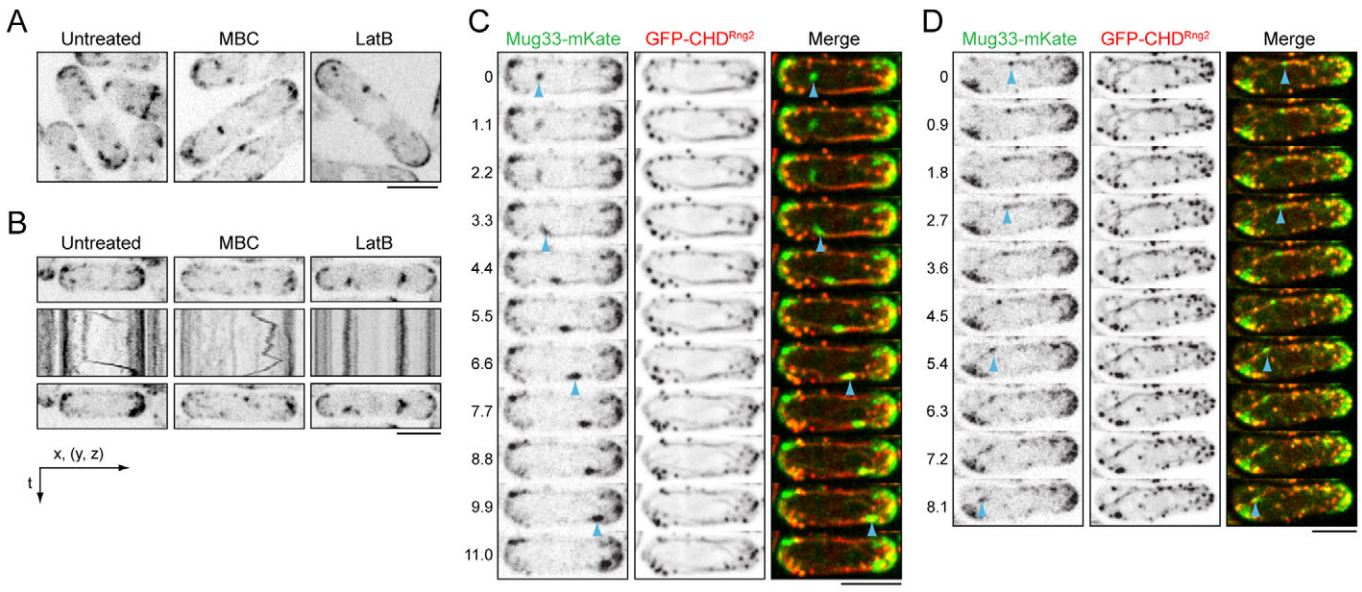

Fig. 3. Mug33 tubulovesicular elements translocate along actin cables. (**A**) Localization of Mug33–GFP in untreated (DMSO control), MBC-treated and LatB-treated wild-type cells. (**B**) Kymographs showing Mug33–mKate TVE translocations or absence of translocations in individual treated or untreated cells; images above and below kymographs show the cells at beginning and end of the kymographs. The horizontal axes of kymographs show combined projection of *y*- and *z*-information along the *x*-axis of images. Vertical axes of kymographs show time; the total time is 67 seconds for untreated cells, 58 seconds for MBC-treated cells and 43 seconds for LatB-treated cells (see Materials and Methods). (**C**,**D**) Time-lapse montage of Mug33–mKate (green) and GFP–CHD^{Rng2} (actin, red) in (C) wild-type cells and (D) *tea1*Δ cells. Arrowheads indicate Mug33 TVEs. The elapsed time is shown in seconds. Scale bars: 5 µm.

overlapping localization at cell tips and did not colocalize in the cytoplasm (supplementary material Fig. S1C). Unlike Tea1 particles, which are dynamically transported towards cell tips by association with growing microtubule plus-ends (Behrens and Nurse, 2002; Feierbach et al., 2004; Snaith and Sawin, 2003), Mug33 cytoplasmic structures showed no colocalization with microtubules (supplementary material Fig. S1D, Movie 1).

Time-lapse imaging revealed that Mug33 cytoplasmic structures were nevertheless dynamic, showing two types of movement: oscillatory behavior over short distances, in apparently random directions; and long rapid vectorial translocation, which was much faster than Tea1 particle movement (~0.34 µm/second for Mug33 compared with ~0.04 µm/second for Tea1; Fig. 3B–D; Table 1; supplementary material Fig. S1C). In wild-type cells, 48% of Mug33 translocations terminated at cell tips, 27% started at cell tips and 25% occurred in the cytoplasm without obvious contact with cell tips (Table 1). Analysis of still and time-lapse images revealed that translocating Mug33 structures were not always discrete puncta, like Tea1 particles, but instead often showed a more extended and sometimes dynamic structure, suggesting deformation under tension (supplementary material Fig. S2, Movie 2). We will therefore refer to the Mug33-containing structures as tubulovesicular elements (TVEs).

The fast movement of Mug33 TVEs persisted after disruption of microtubules with MBC but was abolished upon disruption of filamentous actin with latrunculin B (LatB; Fig. 3A,B; Fig. 4F) suggesting that translocation involves the actin cytoskeleton. Co-imaging Mug33–mKate with actin filaments (GFP–CHD^{Rng2}) showed that Mug33 TVEs associated with and translocated along actin cables, in both wild-type and *tea1*Δ cells (Fig. 3C,D, Fig. 4F; supplementary material Movies 3, 4).

Mug33 TVE translocations were absent in *for3*Δ formin-mutant cells, which specifically lack actin cables as a result of defects in nucleation of the filaments that generate cables (Feierbach and Chang, 2001) (Fig. 4A,B,F; supplementary material Movies 5, 6). In principle, Mug33 TVE movements on actin cables could involve either polymerization-driven mechanisms or motor proteins. For example, in wild-type cells, after nucleating an actin filament,

Table 1. Analysis of Mug33 translocations

Strain	Frequency (events per cell per minute)	Length (µm; ±s.d.)	Speed (µm/second; ±s.d.)	Towards cell tip (%)	Away from cell tip (%)	In cell interior (%)	Total events
Wild-type	1.34	2.91±1.27	0.34±0.17	48	27	25	55
Wild-type, MBC-treated	1.39	3.26±0.91	0.34±0.13	56	25	19	77
tea1Δ	0.87	2.56±1.20	0.21±0.10	47	29	24	75
myo51Δ	0.67	1.85±0.72	0.30±0.14	58	21	21	54
Wild-type, LatB-treated	0	0	0	0	0	0	0
for3Δ	0.089	1.27±0.23	0.09±0.02	0	0	100	4
myo52Δ	0.098	1.56±0.46	0.09±0.02	0	0	100	4

The analysis is based on imaging three *z*-sections at 0.6 µm intervals (combined depth of view equal to ~35–45% of total cell height).

For3 itself is transported centripetally (inwards from the cell tips) at ~0.33 μm/second, which is comparable to the speed of Mug33 translocations, through an actin polymerization-driven mechanism (Martin and Chang, 2006). By co-imaging Mug33–mKate with For3–GFP we found that translocating For3 and Mug33 TVEs did not colocalize on actin cables (Fig. 4C,D). This, together with the fact that ~50% of Mug33 TVE translocations were unambiguously acropetal (towards cell tips), whereas For3 movement is nearly exclusively centripetal (Martin and Chang, 2006), suggested that Mug33 TVE translocations involve more than polymerization-driven movement and are likely to involve motor proteins.

We therefore investigated a role for motor proteins in Mug33 TVE translocations. Fission yeast contains two type V myosins, Myo51 and Myo52. Myo51 has no identified function in the vegetative cell cycle and instead plays a role in meiotic conjugation, cell fusion and spore formation (Doyle et al., 2009; Win et al., 2001). By contrast, Myo52 is important for growth polarity and cytokinesis (Grallert et al., 2007; Martin-Garcia and Mulvihill, 2009; Motegi et al., 2001; Mulvihill et al., 2001; Win et al., 2001). In *myo51*Δ cells, Mug33–GFP was localized at the cell tips and in TVEs, as in wild-type cells, and the frequency, speed and length of TVE translocations was only mildly altered (Fig. 4A,B,F; Table 1). By contrast, in *myo52*Δ cells, Mug33–GFP did not accumulate at the cell tips, and long-range TVE translocations were almost completely abolished, although TVE number and shape were not significantly altered (Fig. 4A,B,F; Table 1; supplementary material Fig. S2). The near-absence of TVE movement in *myo52*Δ was unlikely to be due to defects in actin cable organization, as the dynamics of actin cables and patches appeared relatively normal in this strain, as was also the case for *mug33*Δ mutants (supplementary material Movies 5, 7, 9, 10) (Motegi et al., 2001; Win et al., 2001). We further found that Myo52–GFP colocalized with Mug33–mKate in 100% of TVEs translocating more than 2 μm (*n*=32 translocations analyzed), whereas non-translocating TVEs did not always contain Myo52 (Fig. 4E; supplementary material Movie 11). Taken together, these data demonstrate that Mug33 TVEs translocate along actin cables using the type V myosin motor Myo52.

Mug33 cycling from cytoplasm to the plasma membrane depends on endocytosis and exocytosis

In addition to being required for translocation of Mug33 TVEs, actin filaments were also found to be important for TVE biogenesis itself, as treatment of cells with LatB for prolonged periods (>30 minutes) resulted in a reduction in the number of TVEs, in particular TVEs with extended shape, with a concomitant increase in the amount of Mug33 that was tightly associated with the plasma membrane (Fig. 3A,B; supplementary material Fig. S2). We

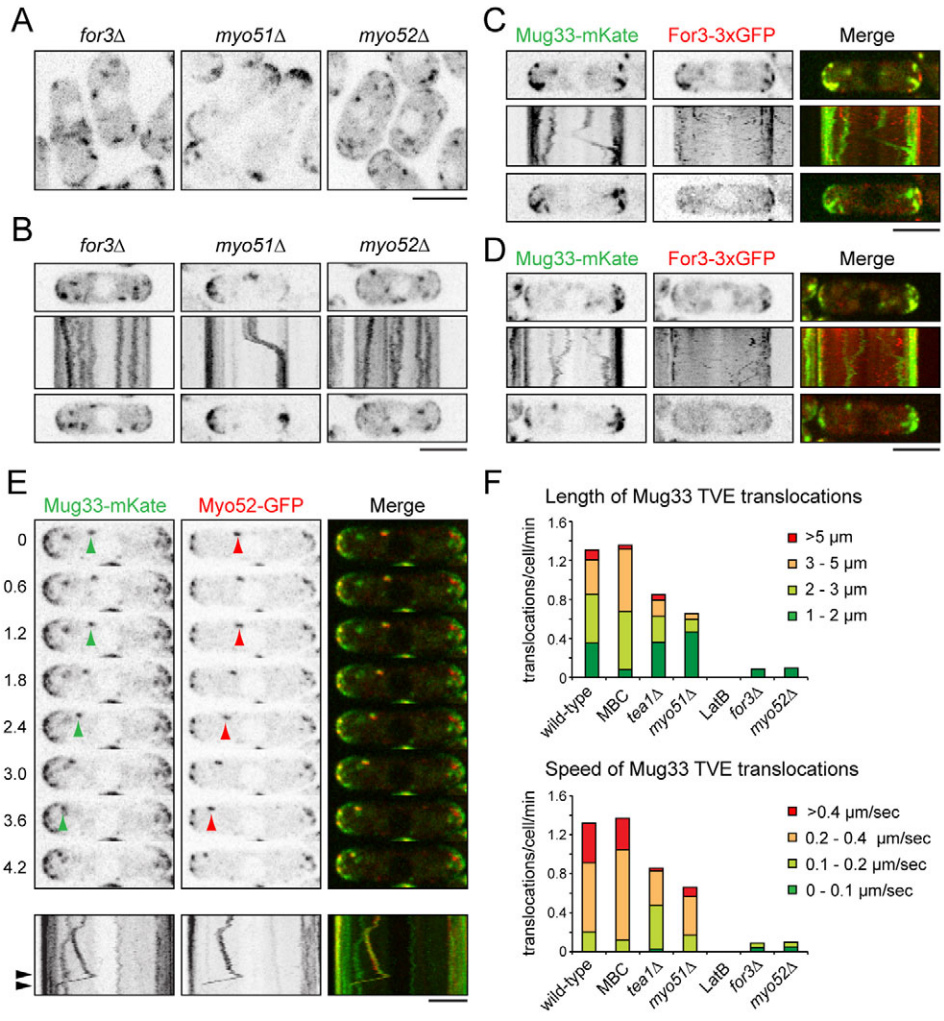

Fig. 4. For3 and Myo52 are required for Mug33 translocation. (**A**) Localization of Mug33–GFP in *for3*Δ and *myo52*Δ cells and Mug33–mKate in *myo51*Δ cells. (**B**) Kymographs showing Mug33–GFP TVE translocations or absence of translocations in individual mutant cells. Kymograph presentation is as in Fig. 3; the total time is 36 seconds. (**C**,**D**) Mug33 and For3 do not co-translocate. Kymographs from single *z*-sections in two wild-type cells coexpressing Mug33–mKate (green) and For3-3xGFP (red); total time is 50 seconds. (**E**) Time-lapse montage and associated kymograph showing co-translocation of Mug33–mKate TVEs (green) with Myo52–GFP (red) in wild-type cells. Green and red arrowheads indicate the same TVE in different channels. The elapsed time is shown in seconds. Kymograph presentation is as in Fig. 3; the total time is 36 seconds. Arrowheads in the kymograph indicate first and last time-points of the montage. (**F**) Length and speed of Mug33 TVE translocations in untreated wild-type, *tea1*Δ, *myo51*Δ, *for3*Δ and *myo52*Δ cells and in wild-type cells treated with MBC and LatB. The different segments within each column indicate the translocation events within the indicated length or speed ranges. See also Table 1. Scale bars: 5 μm.

hypothesized that this was due to disruption of a normal dynamic cycle in which Mug33 transits between TVEs and the plasma membrane. For an integral membrane protein such as Mug33, cycling might be expected to occur through endocytosis and exocytosis, with actin filaments (i.e. in actin patches) being required for endocytosis (Galletta and Cooper, 2009). To investigate whether Mug33 TVEs are formed by endocytosis from the plasma membrane, we examined Mug33 localization relative to that of the lipophilic dye FM4-64, which, upon uptake, inserts into the outer leaflet of the plasma membrane and is rapidly internalized by endocytosis before trafficking to vacuolar membranes (Gachet and Hyams, 2005). Mug33 was present in TVEs that were also labeled with FM4-64, and these translocated through the cytoplasm (Fig. 5A,B).

In budding yeast, Sla2p is a component of actin patches and is required for a late step of endocytosis (Ayscough et al., 1997; Kaksonen et al., 2003). It has been proposed that Sla2p regulates interaction of endocytic proteins with the actin cytoskeleton, perhaps by influencing the timing of Arp2/3-mediated actin filament assembly relative to other endocytic events (Kaksonen et al., 2003). To investigate further the contribution of endocytosis to TVE formation, we examined Mug33 localization in a *sla2*Δ fission yeast mutant (also known as *end4*Δ) (Castagnetti et al., 2005; Iwaki et al., 2004). Extending previous studies of fixed cells (Castagnetti et al., 2005; Iwaki et al., 2004), we found that actin patches in live fission yeast *sla2*Δ cells were less dynamic than in wild-type cells and appeared as 'comet tails' at the plasma membrane that tapered off centripetally, similar to those seen in budding yeast *sla2*Δ mutants (Fig. 5C; supplementary material Movies 5, 8) (Kaksonen et al., 2003). As in LatB-treated wild-type cells, Mug33–GFP in *sla2*Δ cells accumulated on the plasma membrane, and the number of Mug33 cytoplasmic TVEs decreased, especially TVEs with extended shape (Fig. 5D; supplementary material Fig. S2). We also observed occasional transient colocalization of Mug33 and Sla2 (Fig. 5E; supplementary material Movie 12). These results suggest that transit of Mug33 from the plasma membrane to TVEs requires Sla2-mediated endocytosis.

If Mug33 were cycling between TVEs and the plasma membrane, one would also expect Mug33 to be present in exocytic compartments. To investigate this we co-imaged Mug33 with Syb1, the fission yeast homolog of the vesicle SNAREs mammalian synaptobrevin and budding yeast Snc1p, which regulate fusion of exocytic vesicles with the plasma membrane (Baumert et al., 1989; Edamatsu and Toyoshima, 2003; Gurunathan et al., 2000). Mug33 and Syb1 were present in the same TVEs and co-translocated together (Fig. 6A,B). We also found that Mug33 partially colocalized with exocyst subunits Sec6 and Sec8 at cell tips, and some cytoplasmic Mug33 TVEs co-translocated with these proteins (Fig. 6C,D; supplementary material Movies 13, 14). Localization of Sec6, Sec8 and Sec10 was normal in *mug33*Δ cells (Fig. 6E; supplementary material Fig. S3A). However, growth of temperature-sensitive *sec8-1* mutant cells at the restrictive temperature led to the disappearance of Mug33–GFP from cell tips and a reduction in TVEs, despite levels of Mug33–GFP being unaltered (Fig. 6F,G). Mug33 localization was also impaired in cells lacking the exocyst-activating GTPase Rho3 (Fig. 6F). These data indicate that Mug33 colocalizes with the exocyst on exocytic vesicles and that Mug33 depends on an intact exocyst complex for proper localization on TVEs and at cell tips.

Mug33 contributes to exocytosis in a parallel pathway with actin cables

The above results demonstrate that Mug33 is present in both endocytic and exocytic compartments, but they do not indicate whether Mug33 has a role in membrane trafficking or is present only as a cargo. To investigate a functional role for Mug33 in endocytosis, we assayed uptake of FM4-64 in wild-type and mutant cells over time. In *sla2*Δ cells, no uptake of FM4-64 was observed, even over long time-scales (Fig. 7A,D) (Iwaki et al., 2004). By contrast, in both wild-type and *mug33*Δ cells, endocytic vesicles containing FM4-64 were observed as early as 45 seconds after the start of the timecourse, and these accumulated on vacuolar membranes over time (Fig. 7A,D). Similar results were obtained assaying uptake of the fluid-phase endocytic marker Lucifer Yellow (supplementary material Fig. S5) (Riezman, 1985; Takeda and Chang, 2005). We also assayed the rate of exocytosis in *mug33*Δ cells, measuring secretion of acid phosphatase into the culture medium, and found no difference between wild-type and *mug33*Δ

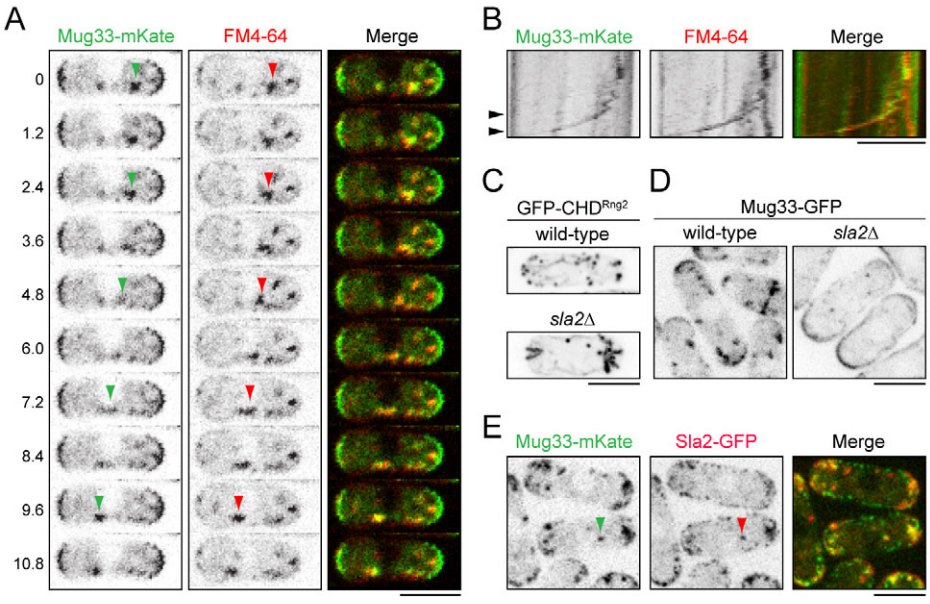

Fig. 5. Mug33 is present in endocytic compartments. (**A**) Time-lapse montage showing co-translocation of Mug33–mKate TVEs (green) with FM4-64 (red) in wild-type cells. Green and red arrowheads indicate the same TVE in different channels. The elapsed time is shown in seconds. Images were acquired ~10 minutes after warming the cells, after prior labeling on ice. (**B**) Kymograph derived from time-lapse acquisition in A; the kymograph presentation is as in Fig. 3; the total time is 30 seconds. Arrowheads indicate the first and last time-points of the montage in A. (**C**) Localization of GFP–CHD^{Rng2} in wild-type and *sla2*Δ cells. (**D**) Localization of Mug33–GFP in wild-type and *sla2*Δ cells. (**E**) Partial colocalization of Mug33–mKate (green) with Sla2–GFP (red) in wild-type cells. Green and red arrowheads indicate the same TVE in different channels. Scale bars: 5 µm.

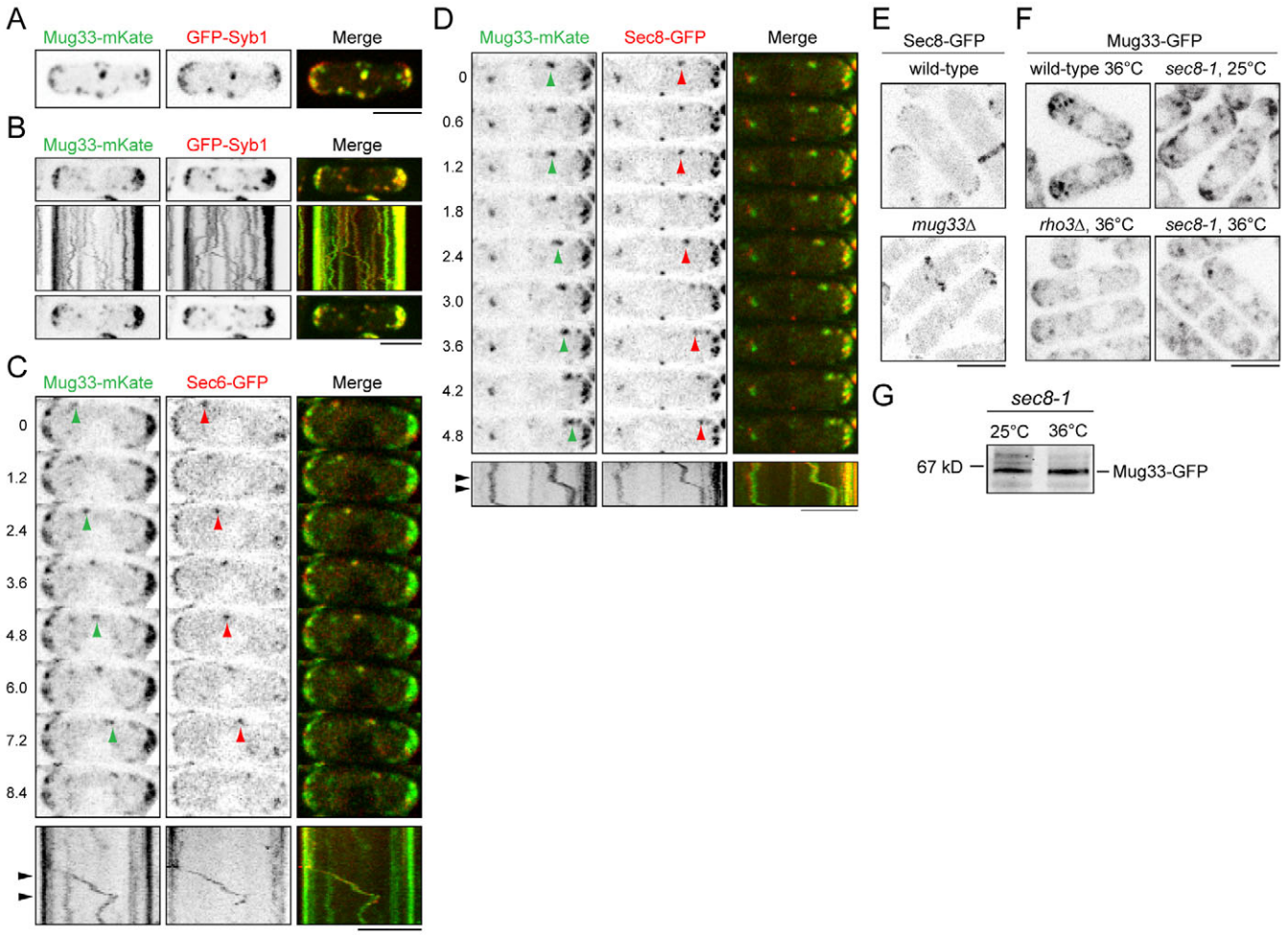

Fig. 6. Mug33 colocalizes with components of the exocytic pathway. (**A**) Colocalization of Mug33–mKate (green) with GFP–Syb1 (red) in a wild-type cell. (**B**) Kymograph of a different wild-type cell, showing co-translocation of Mug33–mKate TVEs with GFP–Syb1. Kymograph presentation is as in Fig. 3; the total time is 96 seconds. (**C**) Time-lapse montage and associated kymograph showing co-translocation of Mug33–mKate (green) with Sec6–GFP (red) in a wild-type cell. Labelling as in Fig. 4E; the total time in kymograph is 36 seconds. (**D**) Time-lapse montage and associated kymograph showing co-translocation of Mug33–mKate (green) with Sec8–GFP (red) in a wild-type cell. Labeling is as in Fig. 4E; the total time in kymograph is 18 seconds. (**E**) Localization of Sec8–GFP in wild-type and *mug33*Δ cells. (**F**) Localization of Mug33–GFP in wild-type cells at 36°C, *sec8-1* at 25°C and 36°C and *rho3*Δ at 36°C. (**G**) Anti-GFP antibody immunoblot of Mug33–GFP in *sec8-1* at 25°C and 36°C. Scale bars: 5 µm.

cells (Fig. 7B). These results suggest that Mug33 is not essential either for efficient endocytosis or exocytosis.

Although deletion of *mug33*$^{+}$ alone did not produce obvious defects in either endocytosis or exocytosis, we wondered whether Mug33 might have a more subtle role in one or both of these processes. We therefore combined *mug33*Δ with non-lethal mutations affecting exocyst function: a temperature-sensitive allele of *sec8* (*sec8-1*), a deletion of non-essential exocyst subunit Exo70, and a deletion of the non-essential exocyst activator Rho3 (Wang, H. et al., 2003; Wang et al., 2002). In addition, we combined all of these mutations with *for3*Δ and *myo52*Δ, as well as *for3*Δ with *myo52*Δ itself (Table 2). Strikingly, we found that a *mug33*Δ *myo52*Δ double mutant was synthetically lethal, and a *mug33*Δ *for3*Δ double mutant exhibited strong synthetic temperature sensitivity (Fig. 7C; Table 2). Moreover, a similar pattern of synthetic interactions was also observed in double mutants combining *exo70*Δ or *rho3*Δ mutations with *for3*Δ or *myo52*Δ. By contrast, *mug33*Δ *exo70*Δ and *mug33*Δ *rho3*Δ double mutants were viable, and *for3*Δ *myo52*Δ double mutants were no more impaired for growth than a *myo52*Δ single mutant (Table 2). Cytologically, *mug33*Δ *for3*Δ and *exo70*Δ *for3*Δ double mutants resembled *for3*Δ mutants, with an increased frequency of lozenge-shaped cells, whereas *mug33*Δ *exo70*Δ double mutants resembled wild-type cells (supplementary material Fig. S4).

The similar genetic interactions of *mug33*Δ, *exo70*Δ and *rho3*Δ mutants with *for3*Δ and *myo52*Δ mutants suggested that Mug33 has a function in exocytosis that is not essential in wild-type cells but becomes important in mutants defective in actin cable-dependent transport. Accordingly, we found that acid phosphatase secretion in *mug33*Δ *for3*Δ double mutants (at 25°C; permissive temperature for growth) was strongly reduced compared with either single mutant (Fig. 7B). A similar synthetic reduction in exocytosis was seen in *exo70*Δ *for3*Δ double mutants. By contrast, and in agreement with cell-viability data, exocytosis in *myo52*Δ *for3*Δ double mutants was the same as in *myo52*Δ single mutants (Fig. 7B).

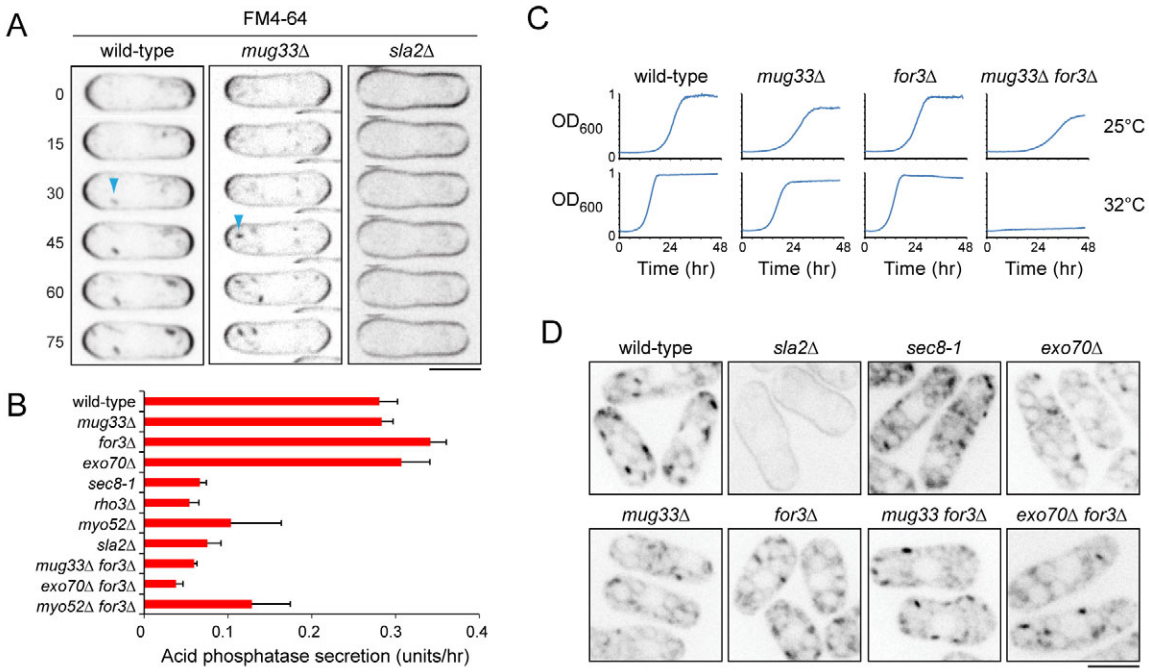

Fig. 7. Mug33 contributes to exocytosis. (**A**) FM4-64 uptake assay in wild-type, *mug33*Δ and *sla2*Δ cells. Cells were labeled with FM4-64 on ice and imaged immediately at room temperature as single *z*-sections. Blue arrowheads indicate nascent endocytic vesicles. (**B**) Rate of acid phosphatase secretion in wild-type and mutant cells. Results are means+s.d. for two independent experiments. (**C**) Growth of wild-type, *mug33*Δ, *for3*Δ and *mug33*Δ *for3*Δ cells at 25°C and 32°C. (**D**) FM4-64 staining in wild-type, *sla2*Δ, *mug33*Δ, *for3*Δ, *sec8-1*, *exo70*Δ, *mug33*Δ *for3*Δ and *exo70*Δ *for3*Δ cells. Cells were first labeled with FM4-64 on ice and then warmed for ~20 minutes at 23°C before imaging as single *z*-sections. Scale bars: 5 μm.

In budding yeast, some mutations affecting endocytosis also affect exocytosis, either directly or indirectly (Goodson et al., 1996; Mulholland et al., 1997; Riezman, 1985). We found that fission yeast *sla2*Δ is defective not only in endocytosis, but also in exocytosis (Fig. 7B). Because *mug33*Δ *for3*Δ mutants showed an exocytosis defect, it was formally possible that the primary defect of *mug33*Δ *for3*Δ was actually in endocytosis. We therefore measured endocytic uptake of FM4-64 and Lucifer Yellow in *mug33*Δ *for3*Δ double mutants and other exocytosis mutants. Whereas *sla2*Δ exhibited no detectable uptake, endocytosis in *mug33*Δ *for3*Δ was comparable both to wild-type cells and to the exocytosis mutants *sec8-1*, *exo70*Δ and *exo70*Δ *for3*Δ (Fig. 7D; supplementary material Fig. S5). Taken together, these data suggest that Mug33 functions with exocyst subunits to promote efficient exocytosis.

Discussion

In this work, we have characterized the in vivo behavior and function of Mug33, a fission yeast transmembrane protein involved in membrane trafficking. Mug33 is a member of the Sur7/PalI family of fungal transmembrane proteins. Budding yeast Sur7p, the prototypical member of this family, localizes to eisosomes/MCC (Brach et al., 2011; Grossmann et al., 2008; Grossmann et al., 2007; Luo et al., 2008; Malinska et al., 2004; Walther et al., 2007; Walther et al., 2006). However, unlike components of eisosomes/MCC, which are static, immobile structures, Mug33 shows dynamic behavior, cycling between the plasma membrane and cytoplasmic TVEs that co-translocate with exocyst subunits along actin cables, using type V myosin Myo52. We expect that Mug33-containing TVEs correspond to endocytic and/or exocytic vesicles and/or compartments, but at present we have not distinguished among these. *Mug33*Δ mutants exhibit the same genetic interactions with *for3*Δ and *myo52*Δ cells as do deletion mutants of regulators of exocyst function (*exo70*Δ and *rho3*Δ), and a *mug33*Δ *for3*Δ double mutant has substantially reduced levels of exocytosis relative to wild-type cells and to either single mutant. We conclude that Mug33 contributes to exocyst-mediated exocytosis.

Table 2. Genetic interactions of *mug33*Δ with mutations affecting actin cytoskeleton and exocyst function

	Single mutant	With *mug33*Δ	With *sec8-1*	With *rho3*Δ	With *exo70*Δ	With *for3*Δ
*mug33*Δ	++++					
sec8-1	++	++				
*rho3*Δ	+++	++	–			
*exo70*Δ	+++	+++	–	+++		
*for3*Δ	+++	–/+	–	–	–/+	
*myo52*Δ	+	–	–	–	–/+	+

++++, normal growth at all temperatures; +++, normal growth at 25°C and 32°C, lethal at 36°C; ++, slightly reduced growth at 25°C and 32°C, lethal at 36°C; +, more reduced growth at 25°C, limited growth at 32°C, lethal at 36°C; –/+, growth at 25°C, lethal at 32°C and 36°C; –, lethal at 25°C, 32°C, 36°C.

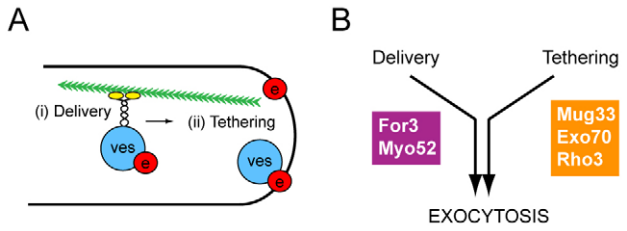

Fig. 8. Two pathways to achieve efficient exocytosis. (**A**) Schematic model of efficient exocytosis involving a combination of frequent delivery of exocytic vesicles (ves, blue) to cell tips, requiring actin cables (green) and type V myosin (yellow), together with tethering of vesicles through an efficiently functioning exocyst complex (e, red). (**B**) Genetic interactions indicate that Mug33, together with Exo70 and Rho3, acts to improve efficiency of exocyst function. See the text for further discussion.

More broadly, our data also suggest a model in which two complementary pathways converge to promote efficient exocytosis in fission yeast (Fig. 8). In this model, the first pathway involves formin-driven nucleation of actin cables and type V myosin-based delivery of exocytic vesicles, whereas the second pathway involves robust exocyst-mediated vesicle tethering, which is dependent on exocyst regulators, including Mug33. In the absence of either individual pathway exocytosis is relatively unaffected, but in the absence of both pathways exocytosis is severely compromised. The main experimental evidence for this model is derived from genetic interactions affecting cell viability or acid phosphatase secretion. Our results place *for3*$^{+}$ and *myo52*$^{+}$ in one genetic-interaction group and *mug33*$^{+}$, *exo70*$^{+}$ and *rho3*$^{+}$ in a second group. Double mutants within a group are relatively non-additive and non-perturbing, whereas double mutants across the two groups are synthetically deleterious.

Our data showing co-translocation of Mug33 TVEs with type V myosin Myo52 and the dependency of Mug33 translocation on Myo52 strongly suggest that translocation of Mug33 TVEs on actin filaments is driven by Myo52. This is similar to post-Golgi trafficking in budding yeast, which depends on the type V myosin Myo2p (Govindan et al., 1995; Pruyne and Bretscher, 2000; Pruyne et al., 1998; Schott et al., 1999). The two types of Mug33 movements we observed – short, random movements and long, vectorial movements – are very similar to those described for GFP-tagged Myo52 itself (Grallert et al., 2007; Motegi et al., 2001). The average speed of Myo52-dependent Mug33 movements in our experiments is slightly lower than that previously described for Myo52 (0.35 µm/second compared with 0.51 µm/second) (Grallert et al., 2007). It is currently unclear whether this is due to minor differences in methodology and/or analysis or to significant differences in biology. One possibility is that Mug33 translocations represent only a subset of total Myo52 translocations and that these have reduced speed. Alternatively, although we observe both acropetal and centripetal co-translocation of Mug33 with Myo52, it is also possible that a subset of Mug33 translocations are driven by actin polymerization, in the manner of (centripetal) For3 translocations, which are generally slower than Myo52-based movement (Grallert et al., 2007; Martin and Chang, 2006); in some instances these might also oppose Myo52-dependent movement. This particular issue would be difficult to address experimentally, because a strong reduction in Myo52-dependent acropetal translocations would lead to reduced Mug33 at cell tips and thus fewer centripetal translocations, even if these did not directly involve Myo52 motor activity. The average speed and frequency of Mug33 translocations in *tea1*Δ cells was also slightly lower than in wild-type cells. This might be due to the fact that although *tea1*Δ has robust actin cables, the number of cables emanating from the non-growing cell tip is reduced (Feierbach et al., 2004); subtle alterations in cable organization in *tea1*Δ cells might also affect the rate of Mug33 translocations.

In principle, if Mug33 function were absolutely dependent on Myo52, one would expect *myo52*Δ cells (which exhibit temperature sensitivity) to be as compromised in growth as *mug33*Δ *myo52*Δ cells (which are synthetically lethal at all temperatures tested). The fact that this is not the case suggests that some Mug33 function is retained without robust acropetal transport; a similar argument applies to the exocyst complex itself, and indeed this is represented in our model (Fig. 8).

At present it is not clear how Mug33 contributes to exocyst function at a mechanistic level. Although Mug33 is present with exocyst components on TVEs and at cell tips, it is unlikely to play a role in exocyst trafficking or localization because steady-state exocyst localization at cell tips is normal in *mug33*Δ cells. Related to this, in preliminary experiments we have found that the intracellular localization and movement of Myo52–GFP and GFP–Syb1 are also unperturbed in *mug33*Δ cells (H.A.S., unpublished data). Because Mug33 is non-essential for viability, while most fission yeast exocyst subunits are essential (Sec5, Sec6, Sec8, Sec10, Sec15, Exo84) (Kim et al., 2010; Wang, H. et al., 2003; Wang et al., 2002), we anticipate that Mug33 is not directly involved in core exocyst function but rather plays a role in regulating core exocyst function, e.g. improving its efficiency. Consistent with this view, exocytosis-defective double mutants such as *mug33*Δ *for3*Δ or *exo70*Δ *for3*Δ did not show significant septation defects, unlike mutants in core exocyst components (supplementary material Fig. S4) (Wang et al., 2002). As one of the key roles of the exocyst is to activate assembly of SNARE complexes and thus membrane fusion (Grote et al., 2000; He and Guo, 2009; Sivaram et al., 2005; Wiederkehr et al., 2004), possible roles for Mug33 could include increasing the stability of the exocyst complex, increasing its residence time on target membranes and/or otherwise enhancing its kinetic ability to activate SNARE complexes. To date we have not identified any physical interactions between Mug33 and exocyst components. Although we initially identified Mug33 as a Tea1-interacting protein, at present it is unclear how or if the interaction of Mug33 with Tea1 is important for exocytosis. In preliminary experiments we have found defects in exocytosis in *tea1*Δ mutants, but additional data suggest that these might not be related to Tea1 localized at cell tips (H.A.S., unpublished data). Further work will be required to clarify this issue.

As is implied in our model (Fig. 8), a better understanding of the regulation of fission yeast exocytosis will require addressing not only Mug33 functions but also how Exo70 functions alongside Mug33 as an exocyst regulator. This is of particular interest because several aspects of exocyst behavior appear to be different between budding and fission yeasts. For example, in budding yeast, the two exocyst subunits Sec3p and Exo70p localize at the plasma membrane independently of the actin cytoskeleton and are thought to provide a target for incoming secretory vesicles carrying the remaining exocyst subunits (Sec5p, Sec6p, Sec8p, Sec10p, Sec15p and Exo84p), whose plasma membrane localization requires active secretion (Boyd et al., 2004; Finger et al., 1998; He and Guo,

2009; He et al., 2007; Zhang et al., 2008). In budding yeast, Exo70p is essential for viability, and Sec3p is essential for viability at elevated temperatures (all other budding yeast exocyst subunits are essential) (Wiederkehr et al., 2003). By contrast, fission yeast Exo70 is essential for viability only at elevated temperatures, and no fission yeast homologs of Sec3p are known to exist (Wang, H. et al., 2003) (our unpublished data). This suggests that fission yeast has evolved alternative strategies to ensure the polarized localization of the exocyst at cell membranes. Accordingly, in preliminary experiments we have found that both Exo70 and Sec8 remain at cell tips in fission yeast after disruption of the actin cytoskeleton with LatB (supplementary material Fig. S3B) (see also Wang, H. et al., 2003; Wang et al., 2002). These differences in details between the two yeasts underscore the potential value of fission yeast as a second yeast model system for exocytosis. Further work on exocytosis in fission yeast will help to illuminate the variety of mechanisms that might modulate core exocyst function.

Materials and Methods

Yeast genetic methods

General yeast methods were as described previously (Moreno et al., 1991). Crosses were performed primarily by tetrad dissection, and all fluorescent-tagged proteins apart from the tubulin marker GFP–Atb2 and the actin marker GFP–CHD^{Rng2} were expressed from endogenous promoters. Genotypes of strains used in this work are presented in supplementary material Table S2. *GFP-CHD^{Rng2}*, *sec8-GFP*, *sec6-GFP*, *sec10-GFP*, *sec8-1* and *rho3*Δ strains were obtained from Mohan Balasubramanian (Temasek Life Sciences Laboratory, National University of Singapore). *Myo52-GFP*, *myo51*Δ and *myo52*Δ were obtained from Dan Mulvihill, University of Kent, UK. *Sla2-GFP* and *sla2*Δ were obtained from Jackie Hayles, CR-UK, London, UK; *For3-3xGFP* was obtained from Sophie Martin, University of Lausanne, Switzerland; and *GFP-Syb1* was obtained from Yoko Toyoshima, University of Tokyo, Japan. The *S. pombe* eisosome/MCC component Pil1 (SPCC736.15) was identified from the fission yeast genome through homology with the *S. cerevisiae* protein (Walther et al., 2006; Zhang et al., 2004). Gene deletion and C-terminal epitope tagging was performed by PCR-based gene targeting, by using the kanMX6 or natMX6 selectable marker for resistance to G418 and nourseothricin, respectively (Bähler et al., 1998; Goldstein and McCusker, 1999; Sato et al., 2009). Hygromycin-resistant strains were constructed as described previously (Anders et al., 2006). Tea1 was tagged with a tandem affinity purification (TAP) tag composed of an S-peptide (Kim and Raines, 1993), a TEV protease cleavage site and a ZZ tag (minimal protein A binding domain) amplified from pKW804 (Brune et al., 2005), a gift from Karsten Weis, University of California, Berkeley, CA. Gene deletions and tagging were confirmed by yeast colony PCR and western blotting as appropriate. Mug33–GFP was judged to be fully functional on the basis of the absence of genetic interactions between *mug33-GFP* and other mutants (data not shown). Mug33–mKate showed identical localization and dynamic behavior to Mug33–GFP and was used primarily in double-labeling experiments with GFP-tagged proteins. We observed some weak genetic interactions between *mug33-mKate* and other mutants (data not shown); this suggests that Mug33-mKate had a partially impaired function, as is often the case for RFP-tagged proteins (Snaith et al., 2010). Quantitative measurements of cell growth rates were performed using a Sunrise microplate reader (Tecan, Switzerland) controlled by Magellan software. Cultures (200 µl) were grown in YE5S in flat-bottomed 96-well plates at a starting OD_{595} of 0.05. Samples were incubated at 25°C or 32°C with shaking, and OD_{595} was measured every 15 minutes for 48 hours.

Purification of Tea1 for mass spectrometric analysis

For two-step purification of Tea1–TAPS (described above), native cell extracts were prepared by freezing pelleted cells in liquid nitrogen and grinding to a powder while frozen. Frozen cell powder (20 g) was resuspended in 40 ml LBN buffer (Gould et al., 2004). Extracts were incubated on ice for 10 minutes, clarified by centrifugation at 3000 ***g*** for 2 minutes at 4°C, and then centrifuged at 50,000 ***g*** for 30 minutes at 4°C. 2×10^9 IgG-coupled Dynabeads, prepared as described previously (Oeffinger et al., 2007), were added to the extract and incubated for 2 hours at 4°C. Beads were washed and incubated with 30 units of TEV protease, prepared as described previously (Lucast et al., 2001), for 2 hours at 4°C as described previously (Gould et al., 2004). S-protein agarose (20 µl) was added to the TEV cleavage supernatant and incubated overnight at 4°C. The beads were washed in WBN (Gould et al., 2004) and incubated in 60 µl 8 M Urea, 50 mM Tris-HCl pH 8.8 at 23°C for 45 minutes.

Mass spectrometric analysis

Digestion

A total of 60 µl of solubilized protein mixture was reduced in 5 mM TCEP at room temperature, alkylated in 10 mM iodoacetamide at room temperature in the dark, and diluted to 2 M urea in 100 mM Tris-HCl pH 8.5. $CaCl_2$ was then added to a final concentration of 1 mM, and samples were incubated for 18 hours at 37°C in the dark with shaking in 0.015 ng/µl trypsin. Samples were neutralized with 13.5 µl 90% formic acid (final concentration 5%), and centrifuged for 30 minutes at 4°C and 21,000 ***g***.

Multidimensional protein identification technology (MudPIT)

After digestion the proteins were pressure-loaded onto a fused silica capillary desalting column containing 3 cm of 5-µm-diameter strong cation exchange (SCX) followed by 3 cm of 5-µm-diameter C18 (reverse phase or RP material) packed into an undeactivated 250-µm internal diameter capillary. The desalting columns were washed overnight in 1.5 ml buffer A (95% water, 5% acetonitrile and 0.1% formic acid). Following desalting, a 100-µm internal diameter capillary of a 10-µm laser pulled tip packed with 10 cm of 3-µm-diameter Aqua C18 material (Phenomenex, Ventura, CA) was attached to the filter union (desalting column–filter union–analytical column) and the entire split-column (desalting column–filter union–analytical column) was placed in line with an Agilent 1100 quaternary HPLC (Palo Alto, CA) and analyzed using a modified six-step separation, as described previously (Washburn et al., 2001). The buffer solutions used were 5% acetonitrile and 0.1% formic acid (buffer A), 80% acetonitrile and 0.1% formic acid (buffer B), and 500 mM ammonium acetate, 5% acetonitrile and 0.1% formic acid (buffer C). The steps were as follows: step 1, 90 minutes gradient from 0–100% buffer B; steps 2–5, 3 minutes of 100% buffer A, 2 minutes of X% buffer C (where X was 20%, 40%, 60% and 80%, respectively, for steps 2–5), a 10 minute gradient of 0–15% buffer B, and a 97 minute gradient of 15–45% buffer B; and step 6, 3 minutes of 100% buffer A, 20 minutes of 100% buffer C, a 10 minutes gradient of 0–15% buffer B, and a 107 minutes gradient of 15–70% buffer B. As peptides eluted from the microcapillary column, they were electrosprayed directly into an LTQ two-dimensional ion trap mass spectrometer (ThermoFinnigan, Palo Alto, CA) with the application of a distal 2.4 kV spray voltage. A cycle of one full-scan mass spectrum (400–1400 *m*/*z*) followed by eight data-dependent MS/MS spectra at a 35% normalized collision energy was repeated continuously throughout each step of the multidimensional separation. Application of mass spectrometer scan functions and HPLC solvent gradients were controlled by the Xcalibur datasystem.

Analysis of tandem mass spectra

As each step was executed, its spectra were recorded to a RAW file and converted into.ms2 format using RawXtract (Version 1.9). Poor quality spectra were removed from the.ms2 dataset using an automated spectral quality assessment algorithm (Bern et al., 2004). Remaining spectra remaining were searched with the SEQUEST algorithm (Eng et al., 1994) against the SGD_S.Pombe (October 2006) protein database concatenated to a decoy database in which the sequence for each entry in the original database was reversed (Peng et al., 2003). All searches were parallelized and performed on a Beowulf computer cluster consisting of 100 1.2 GHz Athlon CPUs (Sadygov et al., 2002). SEQUEST results were assembled and filtered using the DTASelect (version 2.0) program (Cociorva et al., 2007; Tabb et al., 2002) to dynamically set XCorr and DeltaCN thresholds for the entire dataset to achieve a user-specified false positive rate. The complete list of proteins identified by mass spectrometric analysis following two-step purification of Tea1–TAPS is given in supplementary material Table S1.

Immunoprecipitation

For anti-Tea1 antibody immunoprecipitations, native cell extracts were prepared from frozen powder resuspended in buffer LBN. Extracts were clarified by two microfuge centrifugation steps of 900 ***g*** for 5 minutes at 4°C and the concentration adjusted to 20 mg/ml. 1 ml of extract was incubated with 10 µl of protein-G–Sepharose beads non-covalently pre-loaded with 5 µg of affinity purified anti-Tea1 antibody for 2 hours at 4°C. The beads were washed six times in 1 ml of LBN and resuspended in Laemmli sample buffer for SDS-PAGE and western blotting.

Microscopy

Images were acquired at room temperature. DIC and wide-field fluorescent images (Calcofluor and Lucifer Yellow) were collected using a Nikon TE300 microscope equipped with Chroma filters and a 100× 1.4 NA PlanApo objective, using a Photometrics CoolSnap HQ camera and Metamorph software. Other imaging used a Yokogawa spinning disk confocal system (Visitech) using 488 nm and 561 nm lasers, with a Nikon 100× 1.45 NA Plan-Apo objective lens mounted onto a Nikon TE2000 inverted microscope with an Andor Ixon+ DU888 EMCCD camera, controlled by Metamorph software (Bicho et al., 2010). For most double-labeled samples each wavelength was acquired sequentially, except for images in Fig. 4E, Fig. 5A,B and Fig. 6C,D, which were simultaneously imaged with both wavelengths and the signals separated using an Optosplit III image splitter (Cairn Research Ltd, UK). Cells were prepared for live cell imaging by growth at 25°C in minimal medium, mounted onto agarose pads and imaged at 23°C (Snaith et al., 2010). Temperature-sensitive strains to be examined at the non-permissive temperature

were grown at 25°C before shifting to 36°C for 4 hours before imaging using an objective heater (Bioptechs, Butler, Pennsylvania). Microtubules were visualized using derepressed *nmt81*-GFP-Atb2, and actin was visualized using GFP fused to the calponin homology domain of Rng2, under the regulation of the derepressed *nmt41* promoter (Karagiannis et al., 2005; Martin and Chang, 2006; Wang, C. H. et al., 2003). Time-lapse images of Mug33–GFP, Mug33–mKate, Tea1–tdTomato, GFP–CHD^{Rng2}, Sec6–GFP, Sec8–GFP, Sec10–GFP, Myo52–GFP, and GFP–Syb1, Sla2–GFP and Exo70–GFP, contained three *z*-sections at 0.6-µm spacing. Images were acquired with 100, 150 or 200 msecond exposure time per *z*-section, using streaming acquisition mode for wavelength, *z*-position and time (in streaming mode, the time interval between successive time-points depends on the size of the field of view acquired by the camera; as these varied between experiments, intervals between time-points are indicated directly on the relevant figures). Unless otherwise indicated, images are presented as maximum projections. For *z*-series imaging of Pil1–tdTomato and Mug33ΔC–GFP, strains were imaged as nine *z*-sections at 0.5 µm spacing, with a 200 msecond exposure time. Sections 1 and 5 are shown as single *z*-sections ('Top' and 'Middle') and as maximum projections of all nine sections ('All'). For colocalization of Mug33–GFP and Mug33ΔC–GFP with Pil1–tdTomato, colabeled strains were imaged in a single *z*-section with a 200-msecond exposure time. GFP–Atb2 and Mug33–mKate colabeled strains were imaged as five *z*-sections at 0.6-µm spacing every 5 seconds with a 200 msecond exposure time, using streaming acquisition for wavelength and *z*-position only. Shape changes within Mug33–GFP TVEs were imaged as a single *z*-section using streaming acquisition and a 300 msecond exposure time. In experiments involving imaging of Mug33–mKate after drug treatment with Latrunculin B (LatB) or methyl benzimidizole-2-yl carbamate (MBC), cells were treated with 200 µM LatB for 30 minutes or 250 µM MBC for 20 minutes before imaging. LatB and MBC were added to growth media from 100× stock solutions in DMSO. Mug33–mKate was co-imaged with GFP–CHD^{Rng2} to confirm disruption (or preservation) of the actin cytoskeleton. Mug33–mKate For3–3xGFP colabeled strains were imaged in single *z*-sections with a 500 msecond exposure time.

Kymographs were prepared from maximum projections or single *z*-sections (as appropriate), using Metamorph software, by drawing a line through the centre of each cell that was wide enough to include the entire cell (typically 20–28 pixels wide). The speed and length of TVE translocations were determined from kymographs. TVE movements less than 1 µm were excluded from analysis, as these might represent random diffusion. Translocations that might have begun before the start of imaging or finished after the end of imaging were included in analysis; however, these were rare, because translocations are relatively infrequent and are short-lived relative to the duration of time-lapse imaging. Frequency of TVE translocation was determined by counting the total number of translocations >1 µm occurring in >40 minutes of imaging time for each strain or condition.

For FM4-64 labelling, FM4-64 (Invitrogen) was made as a 1.65 mM stock solution in DMSO. Cells were grown in minimal medium, essentially as described previously (Gachet and Hyams, 2005). To co-image Mug33–mKate translocations with FM4-64, the cell pellet from 200 µl of cell culture was resuspended in an equal volume of ice-cold medium, FM4-64 was added to a final concentration of 8 µM and the cells were incubated on ice for 10 minutes. Cells were harvested, washed in 1 ml of ice-cold medium, resuspended in 4 µl of fresh medium, mounted onto a 2% agarose pad and imaged after a ~10 minute incubation at 23°C. Mug33–mKate and FM4-64 were imaged as three *z*-sections at 0.6 µm spacing, with 200 msecond exposure time. To measure the initial rate of FM4-64 uptake, cells were processed as above but imaged as a single *z*-section for FM4-64 immediately after mounting on the agarose pad, at 23°C (imaging every 1 second for 90 seconds). To measure FM4-64 uptake over longer periods cells were grown in minimal medium, concentrated fivefold and incubated in 2 µM FM4-64 for 20 minutes at 25°C and imaged as a single *z*-section directly on a microscope slide (Skau and Kovar, 2010).

Septation and monopolar or bipolar growth were assayed in cells stained for 2 minutes with 5 µg/ml Calcofluor (FB28, Sigma; 5 mg/ml stock solution in DMSO) in 0.1 M PIPES 6.9 pH, 1 mM EGTA, 1 mM $MgSO_4$ buffer and assayed without washing out dye. Cells were imaged directly on glass slides at 23°C in a single *z*-section (200 msecond exposure) using wide-field optics and neutral density filters.

To measure uptake of Lucifer Yellow, 600 µl of a cell culture grown in minimal medium was harvested, the cells resuspended in 30 µl growth medium and Lucifer Yellow CH (Sigma; 40 mg/ml stock solution in water) was added to a final concentration of 4 mg/ml for 30 minutes at 25°C (Riezman, 1985; Takeda and Chang, 2005). Cells were washed three times in 1 ml ice-cold 50 mM sodium phosphate pH 7.5, 10 mM sodium fluoride, 10 mM sodium azide and imaged directly on a glass slide in a single *z*-section using wide-field optics with a Lucifer-Yellow-specific filter set (Chroma) (400 msecond exposure).

Analysis of polarity re-establishment was performed essentially as described previously (Snaith and Sawin, 2003). Cells were grown to the stationary phase for 2 days at 25°C in yeast extract medium (YE5S), diluted 1:20 into fresh medium containing 250 µM MBC (Sigma; 25 mM stock in DMSO) or fresh medium containing DMSO alone (1% DMSO final) and grown at 32°C for 3 hours. The percentage of straight, bent or branched cells in each strain was counted, under bright-field illumination, for n=200 cells per strain per condition.

Acid phosphatase assays

Assays were performed essentially as described previously (Wang et al., 2002). Cells were grown to mid-exponential phase in yeast extract medium (YE5S), washed twice in an equal volume of fresh medium, resuspended at a density of 5×10^6 cells per ml, and incubated at 25°C. 500 µl samples were removed at t=0, 1, 2, 3 and 4 hours; the cells were then pelleted and 300 µl of supernatant added to 300 µl 2 mM para-nitrophenyl phosphate in 100 mM sodium acetate, pH 4.0. Assays were incubated at 30°C for 10 minutes, stopped by the addition of 300 µl 1 N NaOH, and the absorbance read at 420 nm, using the t=0 sample for each strain as the blank. Under these conditions, secretion of acid phosphatase activity was essentially linear over time; therefore measurements for each strain were converted into a single value of secreted units per hour.

We thank M. Balasubramanian, D. Mulvihill, J. Hayles, S. Martin, Y. Toyoshima, and K. Weis for kind gifts of reagents, D. Kelly for technical assistance with image acquisition and analysis, C. Bicho for construction of the Pil1–tdTomato strain, and members of the Sawin laboratory for useful discussions. This work was performed while K.E.S. was a Wellcome Trust Senior Research Fellow in Basic Biomedical Sciences. This work was supported by the Wellcome Trust. Mass-spectrometry was supported by the National Center for Research Resources of the National Institutes of Health by a grant to Trisha Davis (Univ. Washington) entitled 'Comprehensive Biology: Exploiting the Yeast Genome', P41 RR11823. Deposited in PMC for immediate release.

Note added in proof

Independent of our work, two groups have very recently proposed models involving complementary roles for actin cable-dependent transport and exocyst function in fission yeast exocytosis and/or polarized growth (Bendezú and Martin, 2011; Nakano K. et al., 2011).

Supplementary material available online at
http://jcs.biologists.org/cgi/content/full/124/13/2187/DC1

References

Alvarez, F. J., Douglas, L. M., Rosebrock, A. and Konopka, J. B. (2008). The Sur7 protein regulates plasma membrane organization and prevents intracellular cell wall growth in Candida albicans. *Mol. Biol. Cell* **19**, 5214-5225.

Anders, A., Lourenco, P. C. and Sawin, K. E. (2006). Noncore components of the fission yeast gamma-tubulin complex. *Mol. Biol. Cell* **17**, 5075-5093.

Arellano, M., Niccoli, T. and Nurse, P. (2002). Tea3p is a cell end marker activating polarized growth in Schizosaccharomyces pombe. *Curr. Biol.* **12**, 751-756.

Ayscough, K. R., Stryker, J., Pokala, N., Sanders, M., Crews, P. and Drubin, D. G. (1997). High rates of actin filament turnover in budding yeast and roles for actin in establishment and maintenance of cell polarity revealed using the actin inhibitor latrunculin-A. *J. Cell Biol.* **137**, 399-416.

Bähler, J., Wu, J. Q., Longtine, M. S., Shah, N. G., McKenzie, A., 3rd, Steever, A. B., Wach, A., Philippsen, P. and Pringle, J. R. (1998). Heterologous modules for efficient and versatile PCR-based gene targeting in Schizosaccharomyces pombe. *Yeast* **14**, 943-951.

Baumert, M., Maycox, P. R., Navone, F., De Camilli, P. and Jahn, R. (1989). Synaptobrevin: an integral membrane protein of 18,000 daltons present in small synaptic vesicles of rat brain. *EMBO J.* **8**, 379-384.

Behrens, R. and Nurse, P. (2002). Roles of fission yeast tea1p in the localization of polarity factors and in organizing the microtubular cytoskeleton. *J. Cell Biol.* **157**, 783-793.

Bendezú, F. O. and Martin, S. G. (2011). Actin cables and the exocyst form two independent morphogenesis pathways in the fission yeast. *Mol. Biol. Cell* **22**, 44-53.

Bendtsen, J. D., Nielsen, H., von Heijne, G. and Brunak, S. (2004). Improved prediction of signal peptides: SignalP 3.0. *J. Mol. Biol.* **340**, 783-795.

Bern, M., Goldberg, D., McDonald, W. H. and Yates, J. R., 3rd (2004). Automatic quality assessment of peptide tandem mass spectra. *Bioinformatics* **20 Suppl. 1**, i49-i54.

Bicho, C. C., Kelly, D. A., Snaith, H. A., Goryachev, A. B. and Sawin, K. E. (2010). A catalytic role for Mod5 in the formation of the tea1 cell polarity landmark *Curr. Biol.* **20**, 1-6.

Boyd, C., Hughes, T., Pypaert, M. and Novick, P. (2004). Vesicles carry most exocyst subunits to exocytic sites marked by the remaining two subunits, Sec3p and Exo70p. *J. Cell Biol.* **167**, 889-901.

Brach, T., Specht, T. and Kaksonen, M. (2011). Reassessment of the role of plasma membrane domains in the regulation of vesicular traffic in yeast. *J. Cell Sci.* **124**, 328-337.

Browning, H., Hayles, J., Mata, J., Aveline, L., Nurse, P. and McIntosh, J. R. (2000). Tea2p is a kinesin-like protein required to generate polarized growth in fission yeast. *J. Cell Biol.* **151**, 15-28.

Brune, C., Munchel, S. E., Fischer, N., Podtelejnikov, A. V. and Weis, K. (2005). Yeast poly(A)-binding protein Pab1 shuttles between the nucleus and the cytoplasm and functions in mRNA export. *RNA* **11**, 517-531.

Brunner, D. and Nurse, P. (2000). CLIP170-like tip1p spatially organizes microtubular dynamics in fission yeast. *Cell* **102**, 695-704.

Calcagno-Pizarelli, A. M., Negrete-Urtasun, S., Denison, S. H., Rudnicka, J. D., Bussink, H. J., Munera-Huertas, T., Stanton, L., Hervas-Aguilar, A., Espeso, E. A., Tilburn, J. et al. (2007). Establishment of the ambient pH signaling complex in Aspergillus nidulans: PalI assists plasma membrane localization of PalH. *Eukaryot. Cell* **6**, 2365-2375.

Castagnetti, S., Behrens, R. and Nurse, P. (2005). End4/Sla2 is involved in establishment of a new growth zone in Schizosaccharomyces pombe. *J. Cell Sci.* **118**, 1843-1850.

Chang, F., Drubin, D. and Nurse, P. (1997). cdc12p, a protein required for cytokinesis in fission yeast, is a component of the cell division ring and interacts with profilin. *J. Cell Biol.* **137**, 169-182.

Cociorva, D., L. Tabb, D. and Yates, J. R. (2007). Validation of tandem mass spectrometry database search results using DTASelect. *Curr. Protoc. Bioinformatics* **Chapter 13**, Unit 13.4.

Craighead, M. W., Bowden, S., Watson, R. and Armstrong, J. (1993). Function of the ypt2 gene in the exocytic pathway of Schizosaccharomyces pombe. *Mol. Biol. Cell* **4**, 1069-1076.

Denison, S. H., Negrete-Urtasun, S., Mingot, J. M., Tilburn, J., Mayer, W. A., Goel, A., Espeso, E. A., Penalva, M. A. and Arst, H. N., Jr (1998). Putative membrane components of signal transduction pathways for ambient pH regulation in Aspergillus and meiosis in saccharomyces are homologous. *Mol. Microbiol.* **30**, 259-264.

Doyle, A., Martin-Garcia, R., Coulton, A. T., Bagley, S. and Mulvihill, D. P. (2009). Fission yeast Myo51 is a meiotic spindle pole body component with discrete roles during cell fusion and spore formation. *J. Cell Sci.* **122**, 4330-4340.

Edamatsu, M. and Toyoshima, Y. Y. (2003). Fission yeast synaptobrevin is involved in cytokinesis and cell elongation. *Biochem. Biophys. Res. Commun.* **301**, 641-645.

Eng, J., McCormack, A. and Yates, J. (1994). An approach to correlate tandem mass spectral data of peptides with amino acid sequences in a protein database. *J. Am. Soc. Mass Spectrom.* **5**, 976-989.

Feierbach, B. and Chang, F. (2001). Roles of the fission yeast formin for3p in cell polarity, actin cable formation and symmetric cell division. *Curr. Biol.* **11**, 1656-1665.

Feierbach, B., Verde, F. and Chang, F. (2004). Regulation of a formin complex by the microtubule plus end protein tea1p. *J. Cell Biol.* **165**, 697-707.

Finger, F. P., Hughes, T. E. and Novick, P. (1998). Sec3p is a spatial landmark for polarized secretion in budding yeast. *Cell* **92**, 559-571.

Gachet, Y. and Hyams, J. S. (2005). Endocytosis in fission yeast is spatially associated with the actin cytoskeleton during polarised cell growth and cytokinesis. *J. Cell Sci.* **118**, 4231-4242.

Galletta, B. J. and Cooper, J. A. (2009). Actin and endocytosis: mechanisms and phylogeny. *Curr. Opin. Cell Biol.* **21**, 20-27.

Glynn, J. M., Lustig, R. J., Berlin, A. and Chang, F. (2001). Role of bud6p and tea1p in the interaction between actin and microtubules for the establishment of cell polarity in fission yeast. *Curr. Biol.* **11**, 836-845.

Goldstein, A. L. and McCusker, J. H. (1999). Three new dominant drug resistance cassettes for gene disruption in Saccharomyces cerevisiae. *Yeast* **15**, 1541-1553.

Goodson, H. V., Anderson, B. L., Warrick, H. M., Pon, L. A. and Spudich, J. A. (1996). Synthetic lethality screen identifies a novel yeast myosin I gene (MYO5): myosin I proteins are required for polarization of the actin cytoskeleton. *J. Cell Biol.* **133**, 1277-1291.

Gould, K. L., Ren, L., Feoktistova, A. S., Jennings, J. L. and Link, A. J. (2004). Tandem affinity purification and identification of protein complex components. *Methods* **33**, 239-244.

Gourlay, C. W., Dewar, H., Warren, D. T., Costa, R., Satish, N. and Ayscough, K. R. (2003). An interaction between Sla1p and Sla2p plays a role in regulating actin dynamics and endocytosis in budding yeast. *J. Cell Sci.* **116**, 2551-2564.

Govindan, B., Bowser, R. and Novick, P. (1995). The role of Myo2, a yeast class V myosin, in vesicular transport. *J. Cell Biol.* **128**, 1055-1068.

Grallert, A., Martin-Garcia, R., Bagley, S. and Mulvihill, D. P. (2007). In vivo movement of the type V myosin Myo52 requires dimerisation but is independent of the neck domain. *J. Cell Sci.* **120**, 4093-4098.

Gregan, J., Rabitsch, P. K., Sakem, B., Csutak, O., Latypov, V., Lehmann, E., Kohli, J. and Nasmyth, K. (2005). Novel genes required for meiotic chromosome segregation are identified by a high-throughput knockout screen in fission yeast. *Curr. Biol.* **15**, 1663-1669.

Grossmann, G., Opekarova, M., Malinsky, J., Weig-Meckl, I. and Tanner, W. (2007). Membrane potential governs lateral segregation of plasma membrane proteins and lipids in yeast. *EMBO J.* **26**, 1-8.

Grossmann, G., Malinsky, J., Stahlschmidt, W., Loibl, M., Weig-Meckl, I., Frommer, W. B., Opekarova, M. and Tanner, W. (2008). Plasma membrane microdomains regulate turnover of transport proteins in yeast. *J. Cell Biol.* **183**, 1075-1088.

Grote, E., Carr, C. M. and Novick, P. J. (2000). Ordering the final events in yeast exocytosis. *J. Cell Biol.* **151**, 439-452.

Guo, W., Roth, D., Walch-Solimena, C. and Novick, P. (1999). The exocyst is an effector for Sec4p, targeting secretory vesicles to sites of exocytosis. *EMBO J.* **18**, 1071-1080.

Gurunathan, S., Chapman-Shimshoni, D., Trajkovic, S. and Gerst, J. E. (2000). Yeast exocytic v-SNAREs confer endocytosis. *Mol. Biol. Cell* **11**, 3629-3643.

He, B. and Guo, W. (2009). The exocyst complex in polarized exocytosis. *Curr. Opin. Cell Biol.* **21**, 537-542.

He, B., Xi, F., Zhang, X., Zhang, J. and Guo, W. (2007). Exo70 interacts with phospholipids and mediates the targeting of the exocyst to the plasma membrane. *EMBO J.* **26**, 4053-4065.

Hofmann, K. and Stoffel, W. (1993). TMBASE-A database of membrane spanning protein segments. *Biol. Chem. Hoppe Seyler* **374**, 166.

Hsu, S. C., Ting, A. E., Hazuka, C. D., Davanger, S., Kenny, J. W., Kee, Y. and Scheller, R. H. (1996). The mammalian brain rsec6/8 complex. *Neuron* **17**, 1209-1219.

Hsu, S. C., Hazuka, C. D., Foletti, D. L. and Scheller, R. H. (1999). Targeting vesicles to specific sites on the plasma membrane: the role of the sec6/8 complex. *Trends Cell Biol.* **9**, 150-153.

Hsu, S. C., TerBush, D., Abraham, M. and Guo, W. (2004). The exocyst complex in polarized exocytosis. *Int. Rev. Cytol.* **233**, 243-265.

Huckaba, T. M., Gay, A. C., Pantalena, L. F., Yang, H. C. and Pon, L. A. (2004). Live cell imaging of the assembly, disassembly, and actin cable-dependent movement of endosomes and actin patches in the budding yeast, Saccharomyces cerevisiae. *J. Cell Biol.* **167**, 519-530.

Iwaki, T., Tanaka, N., Takagi, H., Giga-Hama, Y. and Takegawa, K. (2004). Characterization of end4+, a gene required for endocytosis in Schizosaccharomyces pombe. *Yeast* **21**, 867-881.

Johnston, G. C., Prendergast, J. A. and Singer, R. A. (1991). The Saccharomyces cerevisiae MYO2 gene encodes an essential myosin for vectorial transport of vesicles. *J. Cell Biol.* **113**, 539-551.

Kaksonen, M., Sun, Y. and Drubin, D. G. (2003). A pathway for association of receptors, adaptors, and actin during endocytic internalization. *Cell* **115**, 475-487.

Kaksonen, M., Toret, C. P. and Drubin, D. G. (2005). A modular design for the clathrin- and actin-mediated endocytosis machinery. *Cell* **123**, 305-320.

Karagiannis, J., Bimbo, A., Rajagopalan, S., Liu, J. and Balasubramanian, M. K. (2005). The nuclear kinase Lsk1p positively regulates the septation initiation network and promotes the successful completion of cytokinesis in response to perturbation of the actomyosin ring in Schizosaccharomyces pombe. *Mol. Biol. Cell* **16**, 358-371.

Kee, Y., Yoo, J. S., Hazuka, C. D., Peterson, K. E., Hsu, S. C. and Scheller, R. H. (1997). Subunit structure of the mammalian exocyst complex. *Proc. Natl. Acad. Sci. USA* **94**, 14438-14443.

Kim, D. U., Hayles, J., Kim, D., Wood, V., Park, H. O., Won, M., Yoo, H. S., Duhig, T., Nam, M., Palmer, G. et al. (2010). Analysis of a genome-wide set of gene deletions in the fission yeast Schizosaccharomyces pombe. *Nat. Biotechnol.* **28**, 617-623.

Kim, J. S. and Raines, R. T. (1993). Ribonuclease S-peptide as a carrier in fusion proteins. *Protein Sci.* **2**, 348-356.

Krogh, A., Larsson, B., von Heijne, G. and Sonnhammer, E. L. (2001). Predicting transmembrane protein topology with a hidden Markov model: application to complete genomes. *J. Mol. Biol.* **305**, 567-580.

Kubler, E. and Riezman, H. (1993). Actin and fimbrin are required for the internalization step of endocytosis in yeast. *EMBO J.* **12**, 2855-2862.

Lucast, L. J., Batey, R. T. and Doudna, J. A. (2001). Large-scale purification of a stable form of recombinant tobacco etch virus protease. *Biotechniques* **30**, 544-6, 548, 550 passim.

Luo, G., Gruhler, A., Liu, Y., Jensen, O. N. and Dickson, R. C. (2008). The sphingolipid long-chain base-Pkh1/2-Ypk1/2 signaling pathway regulates eisosome assembly and turnover. *J. Biol. Chem.* **283**, 10433-10444.

Malinska, K., Malinsky, J., Opekarova, M. and Tanner, W. (2004). Distribution of Can1p into stable domains reflects lateral protein segregation within the plasma membrane of living S. cerevisiae cells. *J. Cell Sci.* **117**, 6031-6041.

Martin, S. G. (2009). Microtubule-dependent cell morphogenesis in the fission yeast. *Trends Cell Biol.* **19**, 447-454.

Martin, S. G. and Chang, F. (2006). Dynamics of the formin for3p in actin cable assembly. *Curr. Biol.* **16**, 1161-1170.

Martin, S. G., McDonald, W. H., Yates, J. R., 3rd and Chang, F. (2005). Tea4p links microtubule plus ends with the formin for3p in the establishment of cell polarity. *Dev. Cell* **8**, 479-491.

Martin-Castellanos, C., Blanco, M., Rozalen, A. E., Perez-Hidalgo, L., Garcia, A. I., Conde, F., Mata, J., Ellermeier, C., Davis, L., San-Segundo, P. et al. (2005). A large-scale screen in S. pombe identifies seven novel genes required for critical meiotic events. *Curr. Biol.* **15**, 2056-2062.

Martin-Garcia, R. and Mulvihill, D. P. (2009). Myosin V spatially regulates microtubule dynamics and promotes the ubiquitin-dependent degradation of the fission yeast CLIP-170 homologue, Tip1. *J. Cell Sci.* **122**, 3862-3872.

Mata, J. and Nurse, P. (1997). Tea1 and the microtubular cytoskeleton are important for generating global spatial order within the fission yeast cell. *Cell* **89**, 939-949.

Mata, J., Lyne, R., Burns, G. and Bahler, J. (2002). The transcriptional program of meiosis and sporulation in fission yeast. *Nat. Genet.* **32**, 143-147.

McCollum, D., Feoktistova, A., Morphew, M., Balasubramanian, M. and Gould, K. L. (1996). The Schizosaccharomyces pombe actin-related protein, Arp3, is a component of the cortical actin cytoskeleton and interacts with profilin. *EMBO J.* **15**, 6438-6446.

Mitchison, J. M. and Nurse, P. (1985). Growth in cell length in the fission yeast Schizosaccharomyces pombe. *J. Cell Sci.* **75**, 357-376.

Moreno, S., Klar, A. and Nurse, P. (1991). Molecular genetic analysis of fission yeast Schizosaccharomyces pombe. *Methods Enzymol.* **194**, 795-823.

Motegi, F., Arai, R. and Mabuchi, I. (2001). Identification of two type V myosins in fission yeast, one of which functions in polarized cell growth and moves rapidly in the cell. *Mol. Biol. Cell* **12**, 1367-1380.

Mulholland, J., Wesp, A., Riezman, H. and Botstein, D. (1997). Yeast actin cytoskeleton mutants accumulate a new class of Golgi-derived secretary vesicle. *Mol. Biol. Cell* **8**, 1481-1499.

Mulvihill, D. P., Pollard, P. J., Win, T. Z. and Hyams, J. S. (2001). Myosin V-mediated vacuole distribution and fusion in fission yeast. *Curr. Biol.* **11**, 1124-1127.
Munson, M. and Novick, P. (2006). The exocyst defrocked, a framework of rods revealed. *Nat. Struct. Mol. Biol.* **13**, 577-581.
Nakano, K., Toya, M., Yoneda, A., Asami, Y., Yamashita, A., Kamasawa, N, Osumi, M. and Yamamoto, M. (2011). Pob1 ensures cylindrical cell shape by coupling two distinct Rho signaling events during secretory vesicle targeting. *Traffic* **12**, 726-739.
Novick, P., Field, C. and Schekman, R. (1980). Identification of 23 complementation groups required for post-translational events in the yeast secretory pathway. *Cell* **21**, 205-215.
Oeffinger, M., Wei, K. E., Rogers, R., DeGrasse, J. A., Chait, B. T., Aitchison, J. D. and Rout, M. P. (2007). Comprehensive analysis of diverse ribonucleoprotein complexes. *Nat. Methods* **4**, 951-956.
Ottilie, S., Miller, P. J., Johnson, D. I., Creasy, C. L., Sells, M. A., Bagrodia, S., Forsburg, S. L. and Chernoff, J. (1995). Fission yeast pak1+ encodes a protein kinase that interacts with Cdc42p and is involved in the control of cell polarity and mating. *EMBO J.* **14**, 5908-5919.
Penalva, M. A., Tilburn, J., Bignell, E. and Arst, H. N., Jr (2008). Ambient pH gene regulation in fungi: making connections. *Trends Microbiol.* **16**, 291-300.
Peng, J., Elias, J. E., Thoreen, C. C., Licklider, L. J. and Gygi, S. P. (2003). Evaluation of multidimensional chromatography coupled with tandem mass spectrometry (LC/LC-MS/MS) for large-scale protein analysis: the yeast proteome. *J. Proteome Res.* **2**, 43-50.
Pruyne, D. and Bretscher, A. (2000). Polarization of cell growth in yeast. I. Establishment and maintenance of polarity states. *J. Cell Sci.* **113**, 365-375.
Pruyne, D. W., Schott, D. H. and Bretscher, A. (1998). Tropomyosin-containing actin cables direct the Myo2p-dependent polarized delivery of secretory vesicles in budding yeast. *J. Cell Biol.* **143**, 1931-1945.
Ren, G., Vajjhala, P., Lee, J. S., Winsor, B. and Munn, A. L. (2006). The BAR domain proteins: molding membranes in fission, fusion, and phagy. *Microbiol. Mol. Biol. Rev.* **70**, 37-120.
Riezman, H. (1985). Endocytosis in yeast: several of the yeast secretory mutants are defective in endocytosis. *Cell* **40**, 1001-1009.
Rupes, I., Jia, Z. and Young, P. G. (1999). Ssp1 promotes actin depolymerization and is involved in stress response and new end take-off control in fission yeast. *Mol. Biol. Cell* **10**, 1495-1510.
Sadygov, R. G., Eng, J., Durr, E., Saraf, A., McDonald, H., MacCoss, M. J. and Yates, J. R., 3rd (2002). Code developments to improve the efficiency of automated MS/MS spectra interpretation. *J. Proteome Res.* **1**, 211-215.
Sato, M., Toya, M. and Toda, T. (2009). Visualization of fluorescence-tagged proteins in fission yeast: the analysis of mitotic spindle dynamics using GFP-tubulin under the native promoter. *Methods Mol. Biol.* **545**, 185-203.
Sawin, K. E. and Snaith, H. A. (2004). Role of microtubules and tea1p in establishment and maintenance of fission yeast cell polarity. *J. Cell Sci.* **117**, 689-700.
Schott, D., Ho, J., Pruyne, D. and Bretscher, A. (1999). The COOH-terminal domain of Myo2p, a yeast myosin V, has a direct role in secretory vesicle targeting. *J. Cell Biol.* **147**, 791-808.
Schott, D. H., Collins, R. N. and Bretscher, A. (2002). Secretory vesicle transport velocity in living cells depends on the myosin-V lever arm length. *J. Cell Biol.* **156**, 35-39.
Scott, B. L., Van Komen, J. S., Irshad, H., Liu, S., Wilson, K. A. and McNew, J. A. (2004). Sec1p directly stimulates SNARE-mediated membrane fusion in vitro. *J. Cell Biol.* **167**, 75-85.
Shcherbo, D., Merzlyak, E. M., Chepurnykh, T. V., Fradkov, A. F., Ermakova, G. V., Solovieva, E. A., Lukyanov, K. A., Bogdanova, E. A., Zaraisky, A. G., Lukyanov, S. et al. (2007). Bright far-red fluorescent protein for whole-body imaging. *Nat. Methods* **4**, 741-746.
Shen, J., Tareste, D. C., Paumet, F., Rothman, J. E. and Melia, T. J. (2007). Selective activation of cognate SNAREpins by Sec1/Munc18 proteins. *Cell* **128**, 183-195.
Sirotkin, V., Berro, J., Macmillan, K., Zhao, L. and Pollard, T. D. (2010). Quantitative analysis of the mechanism of endocytic actin patch assembly and disassembly in fission yeast. *Mol. Biol. Cell* **21**, 2894-2904.
Sivadon, P., Peypouquet, M. F., Doignon, F., Aigle, M. and Crouzet, M. (1997). Cloning of the multicopy suppressor gene SUR7: evidence for a functional relationship between the yeast actin-binding protein Rvs167 and a putative membranous protein. *Yeast* **13**, 747-761.
Sivaram, M. V., Saporita, J. A., Furgason, M. L., Boettcher, A. J. and Munson, M. (2005). Dimerization of the exocyst protein Sec6p and its interaction with the t-SNARE Sec9p. *Biochemistry* **44**, 6302-6311.
Skau, C. T. and Kovar, D. R. (2010). Fimbrin and tropomyosin competition regulates endocytosis and cytokinesis kinetics in fission yeast. *Curr. Biol.* **20**, 1415-1422.
Snaith, H. A. and Sawin, K. E. (2003). Fission yeast mod5p regulates polarized growth through anchoring of tea1p at cell tips. *Nature* **423**, 647-651.
Snaith, H. A., Anders, A., Samejima, I. and Sawin, K. E. (2010). New and old reagents for fluorescent protein tagging of microtubules in fission yeast; experimental and critical evaluation. *Methods Cell Biol.* **97**, 147-172.
Tabb, D. L., McDonald, W. H. and Yates, J. R., 3rd (2002). DTASelect and Contrast: tools for assembling and comparing protein identifications from shotgun proteomics. *J. Proteome Res.* **1**, 21-26.
Takeda, T. and Chang, F. (2005). Role of fission yeast myosin I in organization of sterol-rich membrane domains. *Curr. Biol.* **15**, 1331-1336.
TerBush, D. R., Maurice, T., Roth, D. and Novick, P. (1996). The Exocyst is a multiprotein complex required for exocytosis in Saccharomyces cerevisiae. *EMBO J.* **15**, 6483-6494.
Toonen, R. F. and Verhage, M. (2007). Munc18-1 in secretion: lonely Munc joins SNARE team and takes control. *Trends Neurosci.* **30**, 564-572.
Toshima, J. Y., Toshima, J., Kaksonen, M., Martin, A. C., King, D. S. and Drubin, D. G. (2006). Spatial dynamics of receptor-mediated endocytic trafficking in budding yeast revealed by using fluorescent alpha-factor derivatives. *Proc. Natl. Acad. Sci. USA* **103**, 5793-5798.
Trybus, K. M. (2008). Myosin V from head to tail. *Cell. Mol. Life Sci.* **65**, 1378-1389.
Verde, F., Mata, J. and Nurse, P. (1995). Fission yeast cell morphogenesis: identification of new genes and analysis of their role during the cell cycle. *J. Cell Biol.* **131**, 1529-1538.
Wachtler, V., Rajagopalan, S. and Balasubramanian, M. K. (2003). Sterol-rich plasma membrane domains in the fission yeast Schizosaccharomyces pombe. *J. Cell Sci.* **116**, 867-874.
Walther, T. C., Brickner, J. H., Aguilar, P. S., Bernales, S., Pantoja, C. and Walter, P. (2006). Eisosomes mark static sites of endocytosis. *Nature* **439**, 998-1003.
Walther, T. C., Aguilar, P. S., Frohlich, F., Chu, F., Moreira, K., Burlingame, A. L. and Walter, P. (2007). Pkh-kinases control eisosome assembly and organization. *EMBO J.* **26**, 4946-4955.
Wang, C. H., Walsh, M., Balasubramanian, M. K. and Dokland, T. (2003). Expression, purification, crystallization and preliminary crystallographic analysis of the calponin-homology domain of Rng2. *Acta Crystallogr. D Biol. Crystallogr.* **59**, 1809-1812.
Wang, H., Tang, X., Liu, J., Trautmann, S., Balasundaram, D., McCollum, D. and Balasubramanian, M. K. (2002). The multiprotein exocyst complex is essential for cell separation in Schizosaccharomyces pombe. *Mol. Biol. Cell* **13**, 515-529.
Wang, H., Tang, X. and Balasubramanian, M. K. (2003). Rho3p regulates cell separation by modulating exocyst function in Schizosaccharomyces pombe. *Genetics* **164**, 1323-1331.
Wang, S. and Hsu, S. C. (2006). The molecular mechanisms of the mammalian exocyst complex in exocytosis. *Biochem. Soc. Trans.* **34**, 687-690.
Washburn, M. P., Wolters, D. and Yates, J. R., 3rd (2001). Large-scale analysis of the yeast proteome by multidimensional protein identification technology. *Nat. Biotechnol.* **19**, 242-247.
Wiederkehr, A., Du, Y., Pypaert, M., Ferro-Novick, S. and Novick, P. (2003). Sec3p is needed for the spatial regulation of secretion and for the inheritance of the cortical endoplasmic reticulum. *Mol. Biol. Cell* **14**, 4770-4782.
Wiederkehr, A., De Craene, J. O., Ferro-Novick, S. and Novick, P. (2004). Functional specialization within a vesicle tethering complex: bypass of a subset of exocyst deletion mutants by Sec1p or Sec4p. *J. Cell Biol.* **167**, 875-887.
Win, T. Z., Gachet, Y., Mulvihill, D. P., May, K. M. and Hyams, J. S. (2001). Two type V myosins with non-overlapping functions in the fission yeast Schizosaccharomyces pombe: Myo52 is concerned with growth polarity and cytokinesis, Myo51 is a component of the cytokinetic actin ring. *J. Cell Sci.* **114**, 69-79.
Young, M. E., Karpova, T. S., Brugger, B., Moschenross, D. M., Wang, G. K., Schneiter, R., Wieland, F. T. and Cooper, J. A. (2002). The Sur7p family defines novel cortical domains in Saccharomyces cerevisiae, affects sphingolipid metabolism, and is involved in sporulation. *Mol. Cell. Biol.* **22**, 927-934.
Zhang, X., Lester, R. L. and Dickson, R. C. (2004). Pil1p and Lsp1p negatively regulate the 3-phosphoinositide-dependent protein kinase-like kinase Pkh1p and downstream signaling pathways Pkc1p and Ypk1p. *J. Biol. Chem.* **279**, 22030-22038.
Zhang, X., Orlando, K., He, B., Xi, F., Zhang, J., Zajac, A. and Guo, W. (2008). Membrane association and functional regulation of Sec3 by phospholipids and Cdc42. *J. Cell Biol.* **180**, 145-158.